Investigating Vortex Ring Reconnection in Twin Parallel Pulsed Jets: Influence of Nozzle Spacing and Stroke Ratio

Théo Chevalier

A Thesis

in

The Department

of

Mechanical, Industrial and Aerospace Engineering

Presented in Partial Fulfillment of the Requirements

For the Degree of

Master of Applied Science (Mechanical Engineering) at

Concordia University

Montréal, Québec, Canada

June 2023

CONCORDIA UNIVERSITY

School of Graduate Studies

This is to certify that the thesis prepared

By: **Théo Chevalier**

Entitled: **Investigating Vortex Ring Reconnection in Twin Parallel Pulsed Jets: Influence of Nozzle Spacing and Stroke Ratio**

and submitted in partial fulfillment of the requirements for the degree of

Master of Applied Science (Mechanical Engineering)

complies with the regulations of this University and meets the accepted standards with respect to originality and quality.

Signed by the Final Examining Committee:

_____ Chair

Dr. Ebenezer Ekow Essel

_____ Examiner

Dr. Ebenezer Ekow Essel

_____ Examiner

Dr. Rolf Wuthrich

_____ Thesis Supervisor(s)

Dr. Lyes Kadem

_____ Thesis Supervisor(s)

Dr. Hoi Dick Ng

Approved by _____

Sivakumar Narayanswamy, MASc. Program Director

June 2023 _____

Dr. Mourad Debbabi, Dean

Gina Cody School of Engineering and Computer Science

Abstract

Investigating Vortex Ring Reconnection in Twin Parallel Pulsed Jets: Influence of Nozzle Spacing and Stroke Ratio

Théo Chevalier

Even though interactions between pulsed jets showed great importance in biological fluid transport, they remain poorly described. An experimental piston/cylinder apparatus is designed to produce twin parallel pulsed jets. Using Particle Image Velocimetry (PIV), we investigate how vortex ring reconnection is influenced by nozzle spacings (S/D_0) varying from 1.49 and 3.20 and stroke ratios (L/D_0) between 2 and 4. Velocity and vorticity visualization suggest there is a critical spacing ratio from which the pulsed jets interact. This value is found to be approximately 3. Below 1.5, the vortex rings are already merged at the jet exit. By implementing a vortex core identification method based on the swirling strength criterion, the reconnection point is then localized. The results highlight how important is the effect of the nozzle spacing compared to the stroke ratio, although the influence of L/D_0 increases with the distance between the jets. Finally, time-frequency analyses confirm the highly fast changes in velocity and vorticity observed during reconnection, and emphasize the importance of the reconnection phase in the newly formed structure.

Acknowledgements

Having a positive impact in both my professional and personal life is important to me. After realizing that I could apply my skills to the biomedical field, I got in touch with Dr. Lyes Kadem. I am very grateful for the trust, welcome and support he gave me. I extend my appreciation to Dr. Hoi Dick Ng for his valuable help in this project. You both offered me a great opportunity to discover the world of research.

I am also sincerely grateful to the LCFD members, who all played a role in this adventure. Special thanks to Dr. Wael Saleh for your time, empathy and help in the design and implementation of the experiments. Moreover, I would like to thank Dr. Giuseppe Di Labbio and Dr. Ahmed Darwish for their sound advice.

Finally, I feel privileged to have parents who have always allowed me to blossom, and a sister who has inspired me in many ways. Last but not least, a big thank you goes to my friend Antoine for his unconditional support in all my crazy projects.

Table of contents

List of figures

List of tables

Glossary

U_j	Jet exit velocity (m/s)
D_0	Nozzle diameter (m)
$y_{0.5}$	Jet half width (m)
U_{cl}	Centerline velocity (m/s)
H	Distance between the jet centerline and a wall parallel to the jet axis (m)
Re	Reynolds number
ν	Kinematic viscosity (m^2/s)
S	Nozzle-to-nozzle distance (m)
U_{max}	Maximum velocity (m/s)
x_{cp}	Combining point longitudinal position (m)
x_{mp}	Merging point longitudinal position (m)
U_p	Piston velocity (m/s)
R	Radius of the vortex ring (m)
t	Time (s)
T	Formation time
L	Piston stroke (m)
Γ	Circulation (s^{-1})
Re_Γ	Reynolds number based on the vortex ring circulation
E_{nd}	Dimensionless kinetic energy
Γ_{nd}	Dimensionless circulation
I	Impulse per unit density ($kg \cdot m \cdot s^{-1}$)
Δ	Spacing ratio

C_o	Dimensionless coupling number
Δt	Time interval (s)
ΔX	Displacement (m)
Stk	Stokes number
τ_p	Particle relaxation time (s)
τ_f	Fluid relaxation time (s)
ρ_p	Particle density (kg/m^3)
d_p	Particle diameter (m)
μ	Dynamic viscosity (Pa·s)
L_f	Fluid characteristic length (m)
U_f	Fluid characteristic velocity (m/s)
Q	Second invariant of the velocity gradient tensor
Δ	Discriminant
∇u	Velocity gradient tensor (s^{-1})
$\lambda_2, \lambda_{ci}, \lambda_{cr}, \lambda_r$	Eigenvalues
v_{ci}, v_{cr}, v_r	Eigenvectors
ψ	Mother function
ω_0	Central pulsation (s^{-1})
X_w	Continuous Wavelet Transform function
ω	Vorticity (s^{-1})
ω^*	Normalized vorticity
U_{tr}	Translating velocity (m/s)
X_r	Reconnection streamwise position (m)

Acronyms

AOI	Area Of Interest
AR	Aspect Ratio
CCD	Charge-Coupled Device
CFD	Computational Fluid Dynamics
CMOS	Complementary Metal-Oxide-Semiconductor
CP	Combining Point
CWT	Continuous Wavelet Transform
DNS	Direct Numerical Simulations
ETER	Edge-To-Edge-Repair
LDA	Laser Doppler Anemometer
LES	Large Eddy Simulations
MP	Merging Point
PIT	Particle Image Tracking
PIV	Particle Image Velocimetry
PLIF	Planar Laser Induced Fluorescence
PPI	Points Per Inch
PSP	Polyamide Seeding Particles
RANS	Reynolds-Averaged Navier-Stokes
RMS	Root Mean Square
VR	Vortex Ring

1. Introduction

Over the past decades, the presence of jets in a wide range of industrial processes has highlighted their great engineering importance. They have become a subject of extensive analytical and experimental research for a better understanding and optimization of their applications, such as mixing [1]–[5], propulsion [6]–[9], or cardiac health [10]–[15]. Besides being highly dependent on the boundary and initial conditions, jets can also be in interaction with other nearby ones or generate fascinating structures like vortex rings. The topic of this study is the combination of these two configurations. Indeed, although steady and pulsed jets have been reviewed for more than a century, vortex ring reconnection has still not been fully scrutinized.

1.1 Motivation

Beyond the beauty of observing this phenomenon, enriching our knowledge of vortex ring interactions will allow us to better understand complex flow structures in cardiac applications. For example, in the case of mitral regurgitation, it is often preferred to proceed to a repair. To

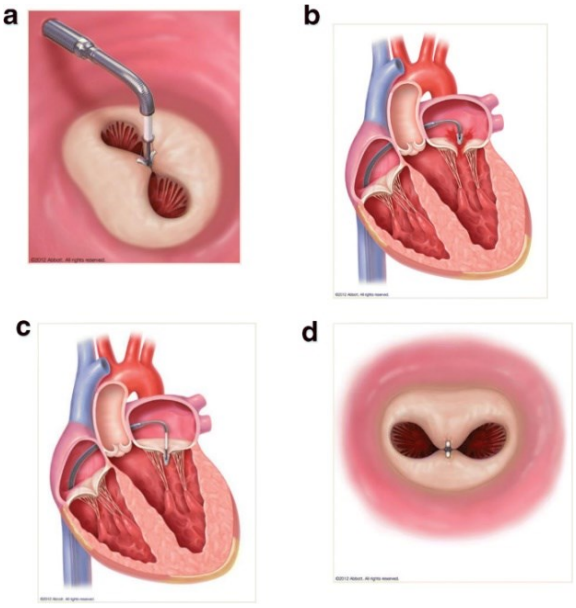

Figure 1.1 The MitraClip system for ETER procedure [16]

do so, one option is to proceed to Edge-To-Edge Repair (ETER), wherein leaflets are attached to each other through a suture or a clip, often positioned in the center or slightly to the side of the center [16]. This leads to a pulsatile jet flow where two vortex rings interact with each other at each beat [15], [17], [18]. An example of such a procedure is presented in Figure 1.1.

Another interesting application is propulsion. As a matter of fact, starting jets can overcome the complex maneuverability at low speeds for underwater robots [6], [19] by reproducing what salps and siphonophores do in nature [20]–[22]. Indeed, these animals can reach high speed efficiently by optimizing and synchronizing their pulses. Figure 1.2 displays an example of such colonial organisms that can be found in nature.

In this study, an experimental investigation on pulsed jet interaction, with a focus on the reconnection of two identical vortex rings evolving side-by-side, is performed. This should allow a better understanding of the impact of such a phenomenon in biological fluid transport.

Figure 1.2 Photo of a siphonophore [23]

1.2 Literature review

In this chapter, the extensive work about steady and pulsed jets through a single or multiple orifices is reviewed, which will allow us to target what may characterize vortex ring interactions.

1.2.1 Steady single jets

It is well-known that a jet can be defined as a pressure-driven fluid flow discharged into a large environment of quiescent fluid. As theorized in [24], a jet stream is generally of a higher momentum than the ambient environment. Jets have the ability of being easily generated while providing efficient mixing by exchanging mass, momentum and heat, particularly in the shear layer. Indeed, the discharge causes instability on its surface, which entails a chaotic motion of eddies across and along the stream. Therefore, a turbulent jet boundary layer of finite thickness appears between the jet fluid flow and the ambient fluid.

Foundations of jet analytical theory are provided by Chaplygin [25] who developed the method of singular points. This method consists in finding all the function's zeros and singularities in the flow region. However, only incompressible fluids were considered. Gurevich [24] expanded the study to any weightless, ideal fluid. Although vorticity is not considered, the author provided one of the first great ranges of analytical results for classical jet flows, with different types of nozzles, and compared them to experimental results.

Even if it should probably be completed with the recent advances in numerical tools, in [26] were reviewed the CFD studies on jets, from the early numerical studies to the Large Eddy Simulations (LES) and Direct Numerical Simulation (DNS) in the 2000s, by way of the Reynolds-Averaged Navier-Stokes (RANS) simulations from 1996. They stated LES is the ideal tool for jet flow simulations in the near future, since numerical researchers are getting a better understanding of the various components involved in LES, and computing power increases.

Furthermore, jets can have many different behaviors depending on numerous parameters. This is what will be investigated in the following.

1.2.1.1 Free steady jets

A free jet is a jet discharged sufficiently far away from any surface or solid boundary. It is the most simple case and has been studied extensively analytically, experimentally and numerically [26]–[30]. The global structure of a free steady jet is well-established [27], [31]. As shown in Figure 1.3, the development of a jet can be decomposed into three regions. Immediately downstream of the nozzle exit, a quasi-laminar flow of constant velocity, called the potential core, appears in the near field. This velocity is equal to the nozzle outlet velocity U_j. The exit velocity distribution normally approaches a 'top-hat' profile, although it depends on the orifice nozzle and is less likely to appear for Reynolds numbers lower than 437 [32]. This zone usually extends up to $4D_0$ to $6D_0$, where D_0 is the diameter of the nozzle exit, depending on the velocity and the fluid properties. Further downstream, the centerline velocity U_{cl} starts to decay, and the shear layer continues to spread into the transitional zone (intermediate field). This region appears when the shear layers of both side merge and can extend up to $20D_0$. Eventually, the flow terminates its progression in the self-similar zone (far field). Further downstream, the centerline velocity decays rapidly, and the jet loses any memory of the nozzle shape. Self-similarity or self-preservation occurs when the velocity decay and jet spread increases almost linearly with distance from the jet exit. In other words, the flow has reached an equilibrium where the dynamical parameters evolve together. A consequence is that the governing equations of the jet flow can be reduced to ordinary differential equation form.

In contact with a stagnant or slower medium, and due to Kelvin-Helmholtz instability, two-dimensional counter-rotating vortices appear and roll up, thereby capturing both the particles of the surrounding fluid and those of the jet on the inner side, thus eroding the potential core.

Consequently, the shear layer develops as large eddies breaking down into smaller eddies. The boundary layer mixes with the ambient fluid, thereby entraining it and increasing the mass flow. The jet width grows approximately linearly on average and symmetrically in the inward and outward directions. The vortices also influence each other, thereby causing vortex stretching or pairing in some cases. While the jet spreads downstream, the centerline velocity decreases to conserve momentum. One can also point out how insignificant the transverse velocity is compared to the longitudinal velocity. This is why the mixing process is so efficient in jet flows [30], [33].

The virtual origin is the source point from which the jet appears to be issuing. The potential core length is generally defined as the distance from the jet exit plane to the point where the centerline velocity decays to ninety percent of the exit jet velocity [34]. The jet half width $y_{0.5}$ corresponds to the distance between the centerline and a transverse plane where the mean velocity becomes half of the associated centerline velocity. It generally increases linearly with x except in regions of axis switching. The spread rate is defined as the slope of the half width line in the

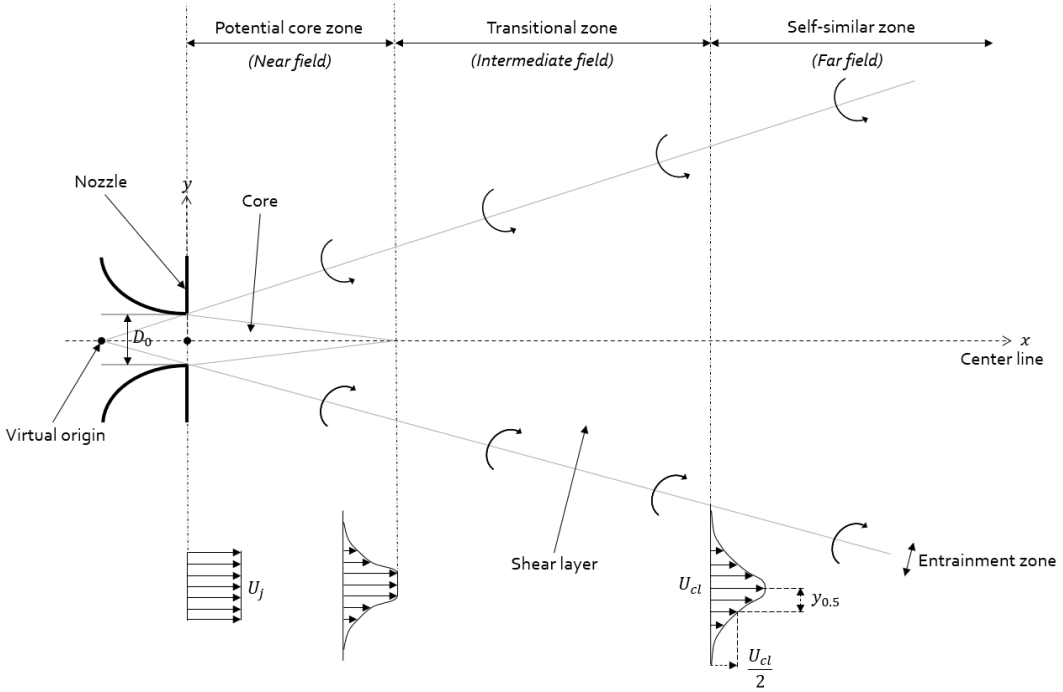

Figure 1.3 Schematic of a free turbulent jet (adapted from [18])

centerline direction. The average size of large eddies is called the integral length scale. Finally, the two other studied scales are the Kolmogorov scale, corresponding to the size of the smallest eddy at which dissipation takes place, and the Taylor micro-scale, which is the size of an intermediate eddy in the energy cascade process.

1.2.1.2 Offset steady jets

An offset jet is a jet discharged into a medium at a certain distance of a wall parallel to the axis of the jet. As schematized in Figure 1.4, this type of flow is characterized by a recirculation region, bounded by the solid boundaries and the dividing streamline, and where a reduced wall pressure causes a deflection of the jet and eventually a reattachment. In this case, an intermediate impingement region follows, and further downstream the flow is similar to a wall jet flow [35], [36]. While approaching the boundary, pressure levels increase, thereby the jet velocity reaches a maximum around the reattachment point and then decelerates.

Bourque and Newman [37] were among the firsts to describe offset jet velocity and pressure behaviors. However, the investigation was simplified by considering the velocity distribution as independent of boundary effects, thus assuming the pressure inside the recirculation zone and the radius of curvature of the jet centerline are constant. Based on the integral formulation of the conservation equations, Rajaratnam and Subramanya [35] developed a theoretical model considering the pressure variations. Later, was proposed a new integral method modified by specifying a polynomial profile for the jet trajectory, in which coefficients are determined by an iterative procedure from boundary conditions, geometric considerations and the approximate momentum relations [36]. Pelfrey and Liburdy [38] provided a detailed study of the mean flow characteristics of a turbulent offset jet in the pre-impingement, recirculation and impingement

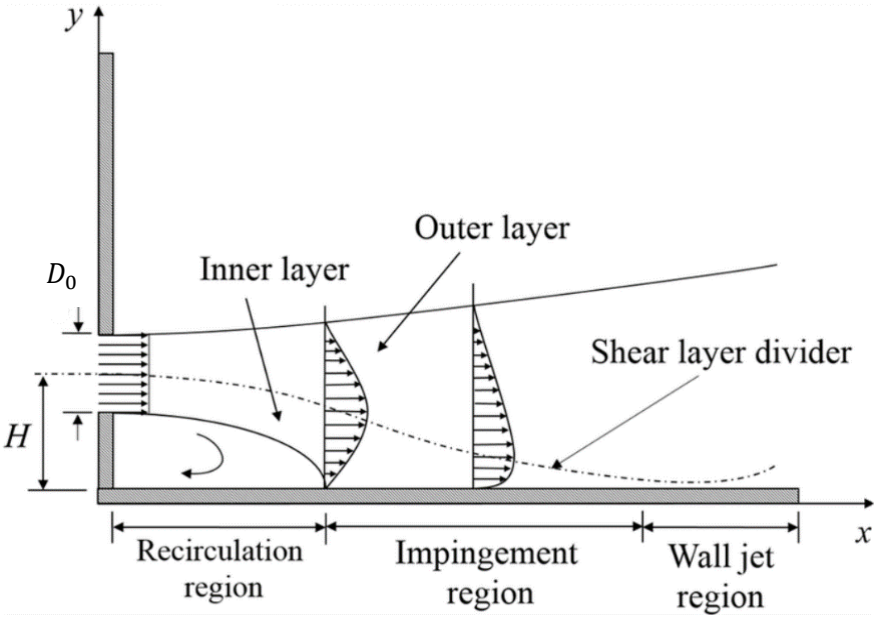

Figure 1.4 Schematic of an offset jet adapted from [137]

regions. They determined that the magnitude of the curvature strain rate is too high to be approximated as a thin shear layer.

The effect of the offset height, or more specifically the offset ratio defined as H/D_0, has been widely studied. Agelin-Chaab [39] studied the effects of offset ratio on the structure of a turbulent round offset jet using Particle Image Velocimetry (PIV) for three Reynolds numbers (5000, 10000 and 20000). It was concluded that the velocity decay and spread rates are nearly independent of the Reynolds number and offset height. However, in [38] was developed a more general uniform relationship between the offset ratio and the reattachment length. The authors put forward that when the Reynolds number is high, the impingement distance only depends on the offset ratio. Assoudi et al. [40] reported measurements of mean velocities and turbulence characteristics, suggesting a higher offset ratio corresponds to a better distribution of the jet within the flow field, and a greater dynamic mixture. Furthermore, the behavior of a three-dimensional turbulent offset jet injected with different densities at various offset heights has been investigated [41]. The study stated that the reattachment length decreases with the increase of the fluid density but increases

with the offset height. Even if no significant impact of these parameters was observed on the decay of the maximum mean velocities in the near region, they observed it was more highly affected downstream of the impingement region. Experimental results on the wall static pressure variation along the offset wall allowed to identify the reattachment point and identify an empirical vortex center relationship. This suggests the flow in the recirculating bubble is similar for different offset ratios [42]. Many other studies on offset jets with offset ratios from 0.694 to 48.5 include measurements of static pressure distributions, mean streamline velocity profiles, and the effect of offset ratio on the streamwise distance of the reattachment point from the nozzle for jets. Nasr and Lai [43] summarized important results before 1998.

1.2.1.3 Wall steady jets

A wall jet is defined as "a boundary layer in which, by virtue of the initially supplied momentum, the velocity over some region in the shear layer exceeds that in the free stream" [44]. One can refer to the aforementioned paper for a review of pre-1980 research on wall jets. A wall jet can be assimilated to an offset jet with a null distance to the parallel wall. The inner layer of a plane wall jet is similar to that of the turbulent boundary layer, while the outer layer is similar to that of a free jet. This was confirmed numerically [45]. George et al. [46] then developed a new theory based on the asymptotic invariance principle in which the outer wall jet is governed by different scaling parameters. This allowed a better description of wall jets, with a focus on the turbulence Reynolds stress. Since it is experimentally difficult to investigate flow characteristics near a boundary, advances in non-intrusive techniques brought new measurement perspectives. Eriksson et al. [47] investigated the inner region of a two-dimensional plane wall jet thanks to Laser-Doppler measurements, providing a new set of data for the wall shear stress. Law and Herlina [48] used a technique combining PIV and Planar Laser Induced Fluorescence (PLIF) to obtain

velocity characteristics. These new results are generally in good agreement with previous studies, while bringing more precision to the measurements. The latter study also provides a summary of the previous investigations on three-dimensional turbulent wall jets.

1.2.2 Influence of boundaries and initial conditions

As the near region is highly turbulent and requires appropriate tools, only the far, self-similar region has first been extensively studied [28], [49]–[52]. Despite this extensive research, some support the idea of a universal self-similar region, independent of the initial conditions [28], [29], [53], whereas others [50], [51], [54] claim there is a wide range of self-similar states, depending on initial conditions, e.g. the exit Reynolds number. Flows can be fully self-preserving at all orders of the turbulence moments and at all scales of motion, or partially preserving, regarding the mean momentum equations, or up to certain orders of the turbulence moments or at certain scales.

Later, advances in imaging techniques such as Particle Image Tracking (PIT) and Velocimetry (PIV), Laser Induced Fluorescence (LIF), or Doppler allowed new perspectives about the near or intermediate fields. These technologies were a turning point in understanding the influence of initial conditions, as described in this section.

1.2.2.1 Effects of the nozzle type

The two main categories of steady single jets are two-dimensional plane jets and axisymmetric round jets. They have different far-field mean centerline velocities: it is approximately proportional to x^{-1} for a round jet and $x^{0.5}$ for a plane jet [27]. For a rectangular jet, the aspect ratio (AR), defined as the ratio of the major axis to the minor axis, generally width and height respectively, has a significant influence on the jet spread. For large AR, this type of jet is free from the effects of side walls and undergoes a phenomenon during which the two axes switch, because of the different

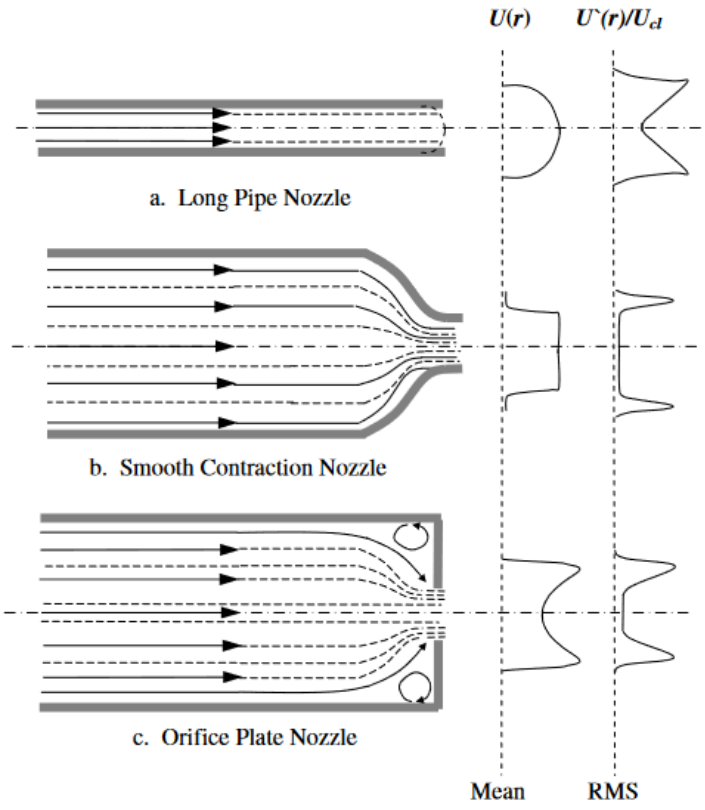

Figure 1.5 Different nozzle shapes commonly studied and their flow characteristics upstream and downstream from the exit [57]

spread rates in the two lateral directions. As round jets are axisymmetric, they do not have this behavior. Deo et al. [55] widely investigated the influence of AR between 15 and 72 on plane jets for a nozzle-height-based Reynolds number of 18000. A higher jet spreading rate was obtained for lower AR. In the near field, an asymptotic profile of the potential core length as the AR increases has been highlighted, while the jet spread rate and centerline velocity decay continue to increase with AR in the far field, which means plane jets do not match with the idea that it becomes independent of the initial conditions at sufficiently large distances from the jet exit.

Furthermore, jets can be generated from different nozzle geometries, like the three common ones presented in Figure 1.5. This has a great influence on the inlet mean velocity profile. Mi et al. [1] compared qualitatively and quantitatively the mixing performance of jets issuing from such

nozzles. They found that a sharp-edged orifice allows the highest mixing rate, while the long straight nozzle has the lowest rate. This is due to different turbulent structures. By comparing a contraction jet and a pipe jet, Xu and Antonia [29] confirmed the first one developed much faster and approached self-preservation more rapidly than the latter. For the pipe jet, they also highlighted that the vortex formation and pairing are disrupted in the shear, while the streamwise vortices, associated with entrainment and turbulent mixing, are absent. Consequently, large-scale structures appear further downstream than for a contraction nozzle. In [56], the flow properties of jets issuing from sharp-edged orifice nozzle and smooth contraction nozzle at high Reynolds numbers were investigated. The authors confirmed the previous results and indicated a 20% reduction of the potential core length for the orifice jet. In addition to this, it was found that the highest value of normalized streamwise turbulence intensity was reached earlier in comparison to a smooth contraction nozzle. Furthermore, the centerline mixing characteristics of nine different cross-sectional nozzle shapes were compared [1]. Jets issuing from a non-circular orifice have a lower potential core average length and a higher mean centerline velocity decay rate than a circular orifice. The orifice with an isosceles triangle orifice seems to involve the greatest mixing rates. This investigation can stimulate more studies on orifice shapes, following industrial applications.

The reader can refer to [58] for a more detailed review of experimental data on incompressible turbulent round jets.

1.2.2.2 Effects of the Reynolds number

The Reynolds number of a jet is defined based on the jet inlet mean velocity, the nozzle diameter (or width for plane jets) and kinematic viscosity ν of the jet fluid as $Re = U_j D_0/\nu$. Thus, this parameter has a direct influence on the turbulent mixing field through viscosity, and an indirect influence through the initial conditions. Zaman [59] has first concluded that round jets are laminar

for Reynolds numbers up to 10^5 and become fully turbulent above. However, a study based on a review of round jets, obtained an asymptotic state showing the critical Reynolds number is about 10^4 [2]. In [60], consistent results were found. Other investigations with a low Reynolds number jet pointed out several flow regimes even in the near region [29], [30]. For example, it was found that below 1600, the flow is laminar with a low energy dissipation, whereas up to 4000, a stronger dissipation indicates a turbulent regime within the shear layer. For higher values, the situation is unstable. An investigation on Reynolds numbers between 1000 and 7000 [61] showed that an increase of the Reynolds number results in a greater turbulence intensity in the near region, and a decrease of the potential core length and the turbulence intensity and diffusion rates, while the jet attains self-similarity significantly earlier. Kwon and Seo [32] used PIV to investigate the effects of Reynolds number in the range from 177 to 5142 on round jets with smooth contraction nozzles. Consistently with previous results, they observed a decrease in the spread rates and the potential core length, and an increase of the Reynolds shear stress levels when the Reynolds number increases. The decay rate was also found to increase up to an asymptotic value reached for $Re = 3208$. A systematic measurement method for the flow field of a plane jet with an aspect ratio of 60 was also developed [62]. Velocity measurements for Reynolds numbers in a range from 1500 to 16500 showed an asymptotic regime up to $Re = 7000$. Up to this asymptotic value, statistical properties of the streamwise velocity field both in the near and far fields showed a great dependence on the Reynolds number. The effect of the Reynolds number was found particularly significant for $Re \leq 10^3$, where the spread rates decrease from 0.14 to 0.10 when Re increases from 1500 to 10000. They also obtained increasing values of the normalized streamwise velocity for an increasing Reynolds number, which refutes the observations made by Namer and Ötügen [61] who

obtained decreasing values. As suggested in [62], this may be due to a common error of consideration between a rectangular nozzle jet (without sidewalls) and a truly plane jet.

1.2.3 Steady double jets

Double jets have been of great interest since the fundamental study by Miller and Comings [63], who compared two-dimensional identical jets issuing from parallel slot nozzles and a single free jet of air at $Re = 10^4$ in the merging region by using a hotwire anemometer and a pressure probe. Tanaka [64], [65] completed this by describing the basic flow patterns and entrainment mechanisms of parallel jets for different nozzle-to-nozzle distances S, or spacing ratio $8.5 \leq S/D_0 \leq 26.3$, and for $4.2 * 10^3 \leq Re \leq 8.75 * 10^3$. Different studies showed interest in double jets with different discharge angles [66], [67], parallel jets of different velocities [68], [69] or parallel to a wall [70], [71]. However, we here focus on twin parallel jets.

Three distinct regions have been identified, as shown in Figure 1.6 [72]. The converging region begins at the nozzle exit and extends to the point where the inner shear layers of the jets merge, termed the merging point, where the velocity on the symmetry plane is equal to zero. The merging lies in a sub-atmospheric pressure region between the jets, resulting in contra-rotating vortices and thereby a negative velocity between the two jets. Therefore, the jets attract each other, with a jet axis coinciding with an arc of a circle. The radius of the jet axis increases with the nozzle distance with a proportional factor of 1.10, except for small spacing ratios, with a critical change around $S/D_0 = 16$. Then, the jets form an intermediate merging region until they reach a combining point, where the two distinct velocity peaks occur to reach a maximum velocity. The super-atmospheric pressure due to the junction of the two jets entails an instability of the flow field that makes measurements more difficult. Finally, the combined region is the region where the flow structure of the combined jets exhibits similar characteristics to that of a self-similar free single jet flow,

although the velocity distribution profiles spread wider and turbulence intensity is larger. The velocity profiles were found to be approximately independent of the spacing ratio, and the momentum flux of the jet in the flow direction is conserved except in the converging region. On the other hand, an investigation of the mixing between two parallel jets found similar results, except for the spread angle of the combined flow which was found slightly lower than that of a single jet [73]. The maximum shear stress was also found similar in both cases. Lin and Sheu [74] qualified the similarities with a single jet by showing that the mean velocity approaches self-preservation in the merging and combined regions, while turbulence intensities and Reynolds stresses in the combined region only. Furthermore, as the turbulence intensity increases, the lateral diffusion characteristics of the jet flow are enhanced, which results in better spreading performance. Ko and Lau [75] focused on the flow structures in the initial region and observed two mixing processes: the pairing of successive vortices which form a coherent structure, and amalgamation where no

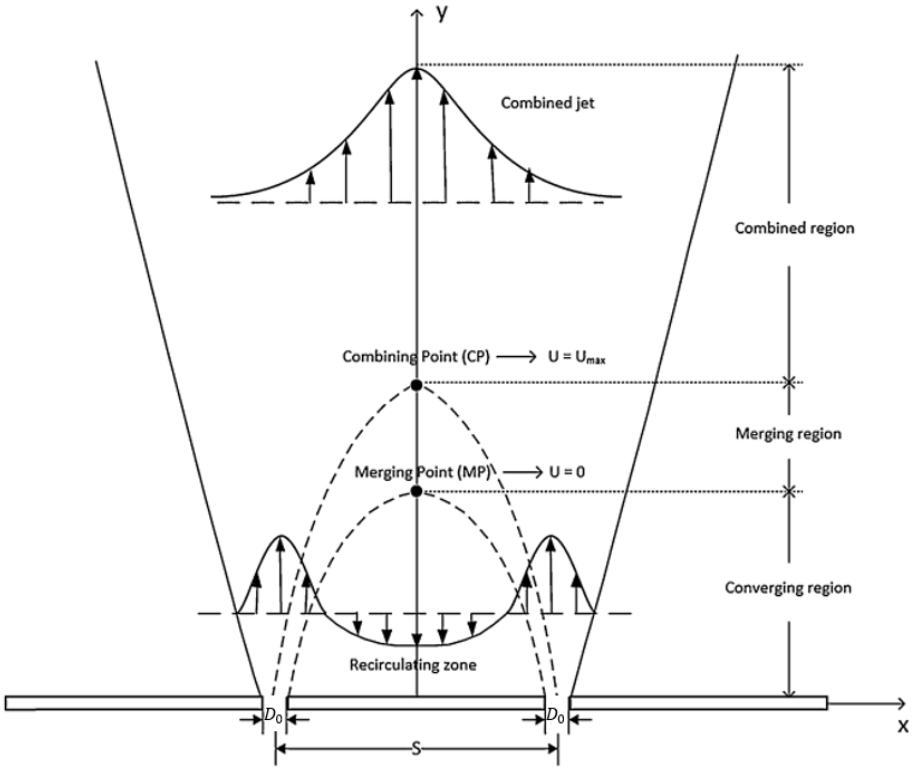

Figure 1.6 Flow structure of parallel rectangular jets [72]

rotational motion occurs, which generates more elongated structures which decay more slowly. In a more recent study, PIV measurements confirmed previous LDA and hot-wire anemometer results for different aspect ratios [72].

As Marsters [76] suggested, the mechanisms of two interacting jets are similar to that of an offset jet. Although Nasr and Lai [43] found common features between the two configurations, significant differences in the combined region were highlighted. Among these, were found a smaller recirculation zone and stronger turbulence intensities in the case of two parallel jets, which suggests that offset jets undergo retarding and turbulence suppression effects on the flow development due to the nearby wall.

Different investigations studied the effects of nozzle spacing and jet Mach number on high-speed dual jets and found results similar to low-speed incompressible jets [77], [78]. The jet flow structure and mixing capacity were found highly influenced by these features, although the latter study focuses on the mean flow field only. Another study performed experiments for Reynolds numbers in the range $3.33 * 10^4 \leq Re \leq 8.33 * 10^4$ and nozzle spacing from 1.5 to 1.89 [3]. An increase of the Reynolds number was found to result in a faster velocity decay, and a higher increase in the combined jet width. It also increases the interference between the two jets, which implies higher Reynolds shear stress and turbulent energy. However, it has no effect on the velocity distributions, which is consistent with Tanaka's findings [64], [65]. On the other side, a higher nozzle spacing tends to decrease the interferences and the velocity and velocity gradient in the mixing region, while it increases the width of the combined jet.

Results were similar for twin round jets [79], [80], with the difference that round jets become close to a single jet further downstream. It also confirmed previous suggestions of a relationship between the nozzle spacing and the merging point [64], [74]. Numerical investigations [4] extended this relationship to the following expression:

$$\frac{x_{cp} - x_{mp}}{D_0} = 0.51 \frac{S}{D_0}$$

where x_{cp} and x_{mp} are the locations of the combined point and merging point, respectively, although it is debatable regarding previous experimental results.

1.2.4 Pulsed jets and vortex rings

1.2.4.1 Vortex ring formation

From smoke rings exhaled from the mouth to industrial waster issuing out of chimneys or squid propulsion, the passion for vortex rings dates back to the classical work by Helmholtz [81]. While he was elaborating on mathematical concepts, Rogers [82] was performing the first experimental work dedicated to the formation of vorticity in a liquid at rest. The formation of vortex rings with the help of jets has then been described by Reusch [83]. In the first half of the XXth century, numerous experimental investigations were performed and summarized in [84]. An even wider state-of-the-art of vortex rings can be found in [85]. Saffman [86] was among the firsts to establish the mathematical foundations of vortex ring formation.

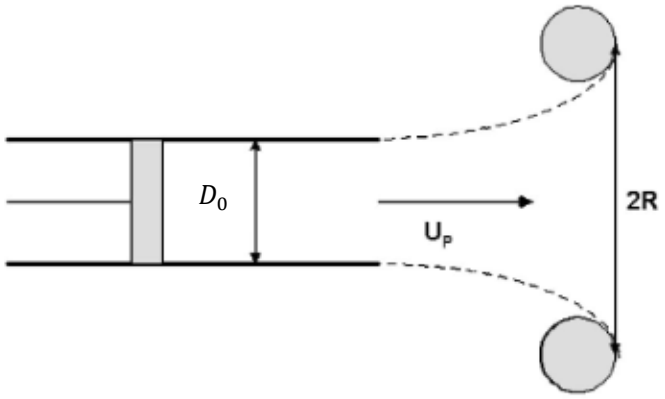

Figure 1.7 Vortex ring formation in a piston/cylinder arrangement [87]

Experimentally, a vortex ring can be generated with a cylinder/piston mechanism, which allows to push a slug of fluid through an orifice or a nozzle. The applied force can be time-dependent in the form of an impulsive, step or ramp function acting at a point or along a line.

Lim and Nickels [67] and, more recently, New and Yu [88] made extensive reviews of the formation process of vortex ring with starting jets. A starting jet is commonly defined as the transient motion produced when a viscous incompressible fluid is forced from an initial state of rest. When the vorticity layers leave the cylinder, jets spread as cylindrical vortex sheets separating at the nozzle exit and rolling up to form a vortex ring, hence evolving downstream with a growing diameter, and entraining the surrounding fluid with a self-induced translational velocity. When the piston stops, a secondary vortex ring of opposite circulation appears. An explanation of this phenomenon lies in the no-slip boundary condition and the induced vorticity generated along the inner wall of the tube. Didden [89] investigated the velocity field, circulation and characteristic diameter of this phenomenon. This highlighted the role of internal and external boundary layers in the formation process and circulation of the vortex ring. Indeed, this secondary vortex is attributed

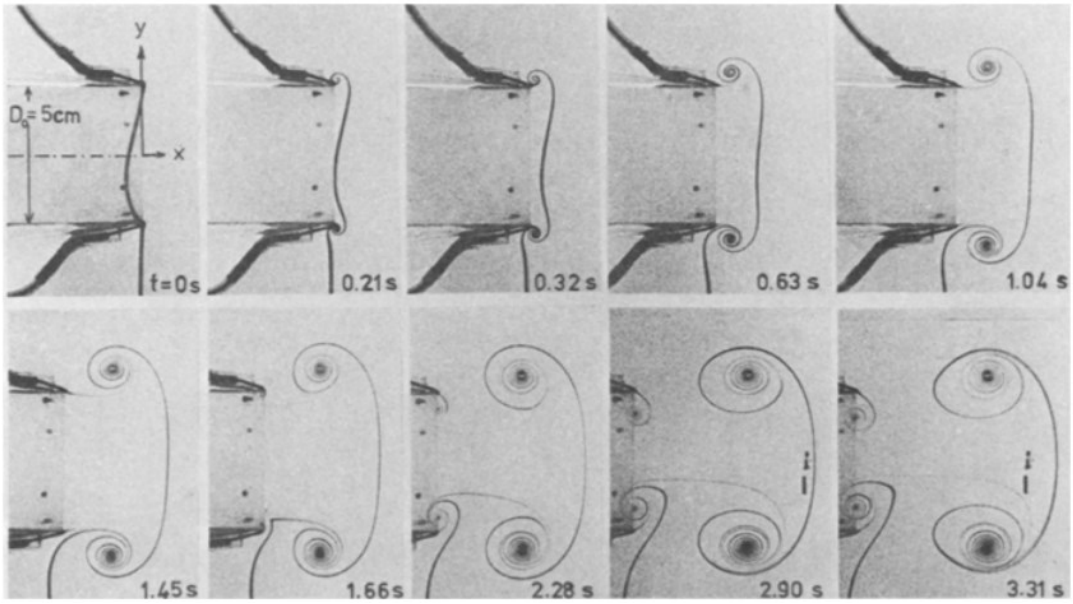

Figure 1.8 Rolling-up process of a vortex ring at a circular nozzle [89]

to the separation and rolling up of the boundary layer produced outside of the cylinder by the induced velocity. Moreover, likewise rectangular steady jets, elliptical vortex rings result in axis switching with a cycle repeating periodically. In [67], the authors showed how significant is the role of the cylinder geometry in the structure of rings, as it can be expected from previous results on steady jets.

The investigation by Gharib et al. [90] has been a reference work in the study of vortex ring formation in a piston/cylinder arrangement. Their goal was to shed light on a limiting process in vortex growth, characterized by a universal time scale called the "*Formation Number*". This critical number corresponds to a limiting value for the stroke ratio, or formation time T, defined by:

$$T = \frac{\overline{U}_p t}{D_0} = \frac{L}{D_0}$$

where

$$\overline{U}_p = \frac{1}{t}\int_0^t U_p(t)dt$$

is the mean velocity discharged at the stop of the piston, t is the time, D_0 is the nozzle diameter and L is the piston stroke, which can be written as:

$$L = \int_0^t U_p(t)dt.$$

The formation number corresponds to the maximum circulation and energy reached by the vortex ring. The most straightforward method to determine the formation number is by comparison of the total circulation discharged by the starting jet and the circulation of the vortex ring after pinch-off. They found that it lies between 3.6 and 4.5, depending on the inlet velocity, the piston velocity, the

exit diameter and the boundaries. For values below this number, individual vortex rings are observed. Above this number, the vortex stops growing and a distinct trailing jet appears. This is called the pinch-off of the jet. It is not sudden as its completion might take up to two formation time units to complete. The existence of such a phenomenon lies in the Kelvin–Benjamin variational principle, which states that steadily translating vortex rings have maximum energy with respect to isovortical perturbations that preserve impulse. Such a maximization principle suggests an optimal pulsing conditions.

Numerical investigations [91]–[93] confirmed experimental and analytical results, including additional cases more complicated to achieve experimentally, which led to the conclusion that the formation time may reach a wider range of values by changing the piston velocity during the stroke, or blunting the inlet velocity profile to a parabolic profile. They also confirmed the existence of a maximum in the circulation a vortex ring can reach with an increase in the stroke ratio. Zhao et al. [92] suggested that the variation in vortex ring circulation may be due to the interaction of the trailing jet instability with the leading vortex ring, concluding the interaction accelerates the pinch-off process. However, another study suggested it is rather due to the shear layer thickness, a thicker layer involving a thicker core size, thus resulting in a slower translational velocity and higher vorticity in the leading vortex ring [93]. Furthermore, in [91] was highlighted a weak dependence of the formation number on the discharge velocity profile or velocity program, although the total circulation is approximately proportional to $\overline{U}_j^2$ and depends on the velocity program. Indeed, a non-uniform velocity program tends to decrease the formation number, while a non-impulsive velocity program results in its increase. If these studies confirmed the findings displayed in [90] and showed that an increase in the Reynolds number is associated with an increase in the formation number, Auerbach [94] found for a pipe jet independence of entrainment properties on this

parameter in the range $3000 < Re < 49000$, which is not the case for orifice nozzles. The author also found that for a constant piston velocity, more fluid is entrained by a pipe jet than by an orifice jet. Eventually, an increasing piston velocity entrains less fluid while a decreasing piston velocity entrains more fluid, although it is less significant. For $1500 \leq Re \leq 4500$, the final diameter reached by a vortex ring induced by a pulsed pipe jet depends on the piston displacement according to the following relationships [95]:

$$\frac{D}{D_0} = 1.18\left(\frac{L}{D_0}\right)^{\frac{1}{3}} \; for \; 0.3 \leq \frac{L}{D_0} \leq 1$$

$$\frac{D}{D_0} = 1.18\left(\frac{L}{D_0}\right)^{\frac{1}{5}} \; for \; 1 \leq \frac{L}{D_0} \leq 3.3$$

For vortex rings induced by an orifice jet over the same range of Reynolds number, the relationship is:

$$\frac{D}{D_0} = 1.05\left(\frac{L}{D_0}\right)^{\frac{1}{4}}$$

These results are consequently independent of the range of Reynolds numbers considered here. It is also worth noting that a Reynolds number based on the vortex ring circulation can be defined by:

$$Re_\Gamma = \frac{\Gamma}{\nu}$$

Based on the slug model (which was questioned later), Mohseni and Gharib [96] suggested that the formation time only depends on the dimensionless kinetic energy per unit density E_{nd} and circulation Γ_{nd} defined as follows:

$$E_{nd} = \frac{E}{\Gamma^{\frac{3}{2}} I^{\frac{1}{2}}}$$

$$\Gamma_{nd} = \frac{\Gamma}{U_p^{\frac{2}{3}} I^{\frac{1}{3}}}$$

where I is the impulse per unit density. This way, they developed an analytical model predicting the dimensionless energy and circulation fall in the range $0.27 \leq E_{nd} \leq 0.4$ and $1.77 \leq \Gamma_{nd} \leq 2.07$ respectively, which was in good agreement with the work of [90].

Moreover, some biological flows were found to meet the maximization condition associated with the formation number. For example, in cardiac flows, vortex ring formation during left ventricle rapid filling is claimed to be an optimized mechanism for blood transport [10], [97], [98]. Another study aimed to improve the model by studying the dynamics of confined and unconfined vortex rings in dense suspensions to model the presence of blood cells [99].

1.2.4.2 Vortex ring interactions

Numerous studies [67], [84]–[86], [100]–[103] showed that, when two identical coaxial vortex rings travel in the same direction, it could lead to a process often referred to as leapfrogging of vortex rings. Other researchers investigated vortex ring head-on collisions, and more particularly the mixing process [5], [104]–[108].

Although these are very fascinating phenomena, the present study focuses on vortex ring reconnection, firstly investigated in [109] with vortex tubes. The latter presented an analytical work on the sinusoidal instability in a pair of counter-rotating vortex tubes shed from the wingtips of an airplane. However, the investigation focuses on the early stages of the interaction. In the animal world, salps and siphonophores synchronize jet strength and timing as colonies to execute precise maneuvers and reach high speed efficiently [20]–[22]. This inspired various works on vortex

reconnection. With the advance of numerical simulation, numerous simulations were performed [110]–[112] to model the phenomenon. They found that, similarly to parallel steady jets, the low pressure which develops between the two vortex rings causes their distortion, which entails a rearrangement of vorticity. It is worth noting that this rearrangement happens much faster than for estimation for viscous transport. This is why the flow is often called inviscid in the case of vortex rings. Kida and Takaoka [113] and Sullivan et al. [114] synthesized the existing literature to develop a mathematical description of the vortex ring reconnection. The reconnection phenomenon was decomposed into several sequences. First, as the two vortex rings get closer, the shape of the vortex core is deformed. This is what is called the head-tail structure. Later, vorticity reconnection happens in an interaction zone where there is a viscous cancellation of oppositely signed vorticity. A cross-linking, also called bridging, is then entailed by the advection of a complex three-dimensional velocity field. Finally, vorticity stretching results in a change in global topology.

As pulsed jets can generate more thrust than an equivalent steady jet [115], Athanassiadis and Hart [6] investigated how the distance between two pulsed jets could influence the resulting thrust. They observed that when the nozzle spacing decreases, thrust and efficiency also decrease according to $1 - C_o\Delta^{-6}$, where $\Delta = S/D_0$ is the spacing ratio and $C_o = 2.04 \pm 0.11$ is a dimensionless coupling number that describes how strongly the two nozzles interaction affects thrust and efficiency. Finally, Sargordi et al. [15] investigated the flow structure of twin parallel pulsed jets in the case of an edge-to-edge procedure for mitral valve repair, which is medically performed to overcome mitral valve regurgitation. They compared the energy dissipation and time-frequency spectra of three configurations and concluded that the symmetric double orifice configuration leads to a sub-optimal performance compared to the single orifice and asymmetric orifice configurations.

1.3 Objectives of the present study

The structures of steady jets and vortex rings have been extensively reviewed for more than 150 years. The discovery of the existence of a universal limiting value for the formation time, the so-called formation number, has been a breakthrough in the understanding of vortex ring formation. More recently, some researchers started studying experimentally and numerically the interactions between two vortex rings. However, these investigations are often limited to the formation of the vortex rings or in the near-field wake, and rarely consider the influence of the nozzle spacing. Therefore, the purpose of this study is to overcome the lack of knowledge covering the reconnection region of two identical vortex rings. More particularly, the intent is to investigate the influence of the nozzle spacing and the stroke ratio on vortex ring interactions using the PIV technique. This will allow a better understanding of the structure of the flow in various fields, especially for cardiac and propulsion applications. To do so, classical measures, such as velocity and vorticity, as well as more advanced techniques, like vortex core identification and Continuous Wavelet Transform (CWT), are used to characterize the dynamics of the interaction of two jets produced through a double piston/cylinder apparatus.

2. Methodology

Experiments carried out in the present study aim to reproduce twin vortex rings spaced by different nozzle spacings S/D_0, and generated by a double piston/cylinder mechanism with several stroke ratios L/D_0. This chapter is devoted to the description of the experimental setup and procedure, as well as data post-processing and treatment.

2.1 Experimental apparatus

The experimental setup consists of a 27.8-cm by 61-cm by 91-cm transparent Plexiglas rectangular water tank, and an electromagnetically driven linear motor (LinMot PS01-37x120) connected to two pistons through a rigid piece of metal that allows to drive the pistons parallel to each other. This plate is clamped to the water tank. The linear motor is fixed to metal beams, themselves fixed to the water tank. The camera is fixed on a tripod and adjusted with a level. A schematic of the setup is shown in Figure 2.1. Although they are not shown in the schematic for simplicity, fixing and supports ensure the stability of the system. The parallelism and alignment of the system were also checked thanks to levels and several preliminary tests.

The flow is driven vertically through 30.5-cm long pipes with an inner diameter of 24.5 mm. The outer diameter is 30 mm, hence a minimum spacing ratio of 1.22. The nozzle exit was sharpened so that the thickness of the pipes does not influence the vortex ring formation. The laser and recording systems are controlled by a computer, while the linear motor is controlled by a second computer.

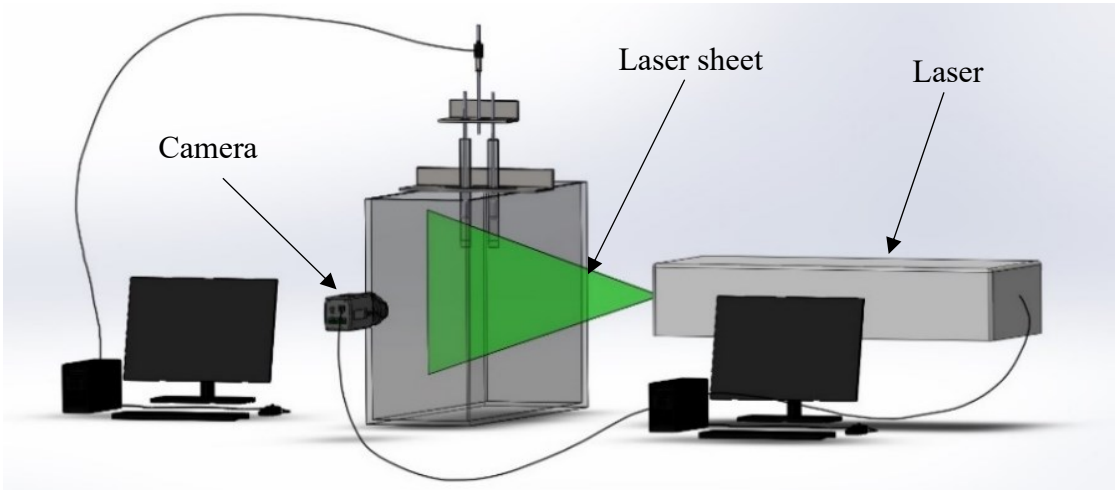

(a)

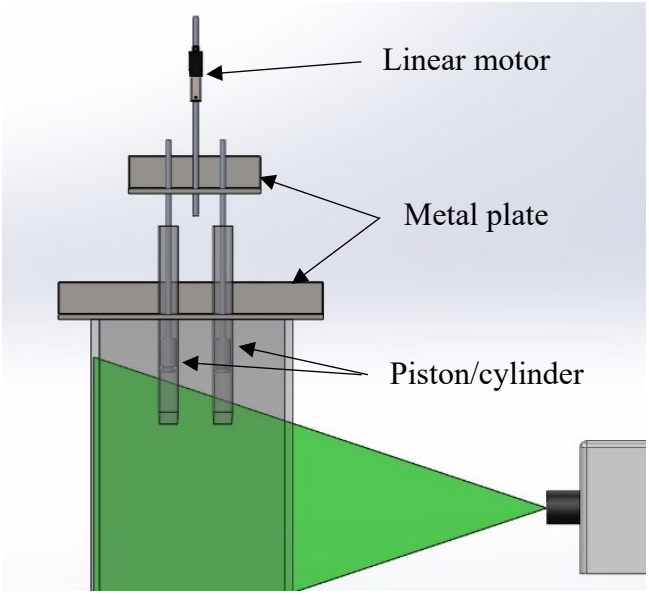

(b)

Figure 2.1 The experimental setup: (a) full view; (b) side view, close up of the piston/cylinder mechanism

2.2 Experimental procedure

Several configurations including four stroke ratios varying from 2 to 4 and seven nozzle spacings varying from 1.94 to 3.20 have been investigated. The values are displayed in Table 2.1. To generate the pulsed jet flow, the piston movement is controlled by the LinMot-Talk software.

The piston stroke movement is an impulse signal with a constant velocity of 15 cm/s. Figure 2.2 displays a recording of the position of the motor arm compared to the ordered position during a stroke with a stroke ratio of 2. Although a slight difference inferior to 0.5 mm was observed, the linear motor response is very satisfactory.

The distance between the piston face and the cylinder exit at a maximum stroke was adjusted to prevent ingestion, which results in an increased ring pulse and an altered trajectory [116]. The Plexiglas tank was filled with room-temperature water and Polyamide Seeding Particles (PSP). The pipes are partially submerged so that their exits are far enough from the free surface. The camera was connected to a synchronizer to link it to the laser and the computer with the recording software. The laser sheet is aligned with the center of the two pipes.

With a jet exit velocity of 15 cm/s assumed to be equal to the piston velocity, a density of 997 kg/m^3 and a viscosity of 10^{-3} Pa·s, the Reynolds number at the exit of the pipe is 3664.

S/D_0	L/D_0
1.49	
1.74	2
1.97	3
2.19	3.5
2.45	4
2.82	
3.20	

Table 2.1 Experimental values of nozzle spacing S/D_0 and stroke ratio L/D_0

2.3 Flow velocity measurement

The PIV optical measurement technique is here used to visualize and analyze the flow. The main components of the PIV setup are a charge-coupled device (CCD), or a complementary metal-oxide-semiconductor (CMOS) camera, a laser and a flow seeded with tracer particles. The latter should have a density equal to that of the fluid, so that they are neutrally buoyant. This technique allows a non-intrusive flow velocity measurement by tracking the motion of particles illuminated with a double-pulsed laser sheet in a planar test section of the experiment. Images are captured at different times with a high-speed camera, therefore allowing to determine the displacement of the particles. The velocity vectors are then calculated by comparing the positions of the particles in each frame. In this study, the laser used for the PIV measurements was a double-pulsed Nd:YLF laser (LDY301, Litron Lasers Ltd.), emitting 100 ns pulses of coherent light of wavelength 527 nm with a frequency of 0.2-20 kHz. The high-speed dual frame CCD camera was the Phantom v9.1, with a Nikon AF Micro-Nikkor 60 mm f/2.8D lens. DaVis 8.4 software by LaVision was used for

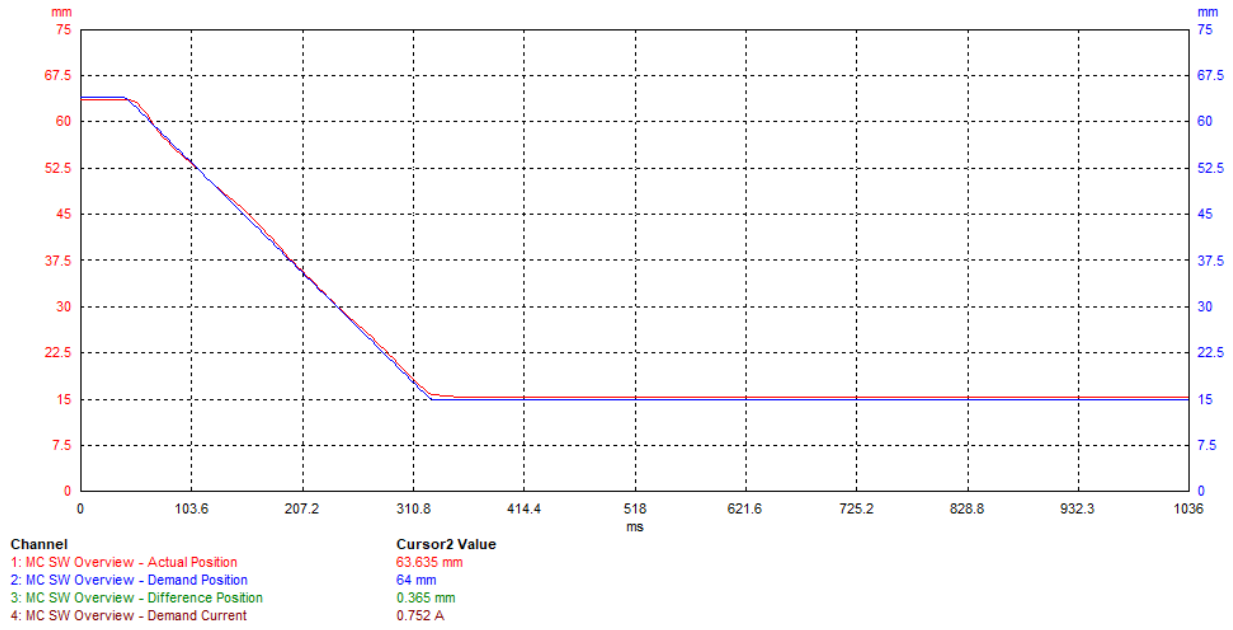

Figure 2.2 Recording of the linear motor position compared to the demand position, for a stroke ratio of 2

recording. The data collected directly from the camera were images in DaVis' own image format '*.im7*', containing tracer particle locations, and were then processed using cross-correlation techniques to obtain vector fields. Then, the data was exported into file format '*.vc7*', and further processed using MATLAB R2020b.

The image analysis is a statistical method, based on the examination of a double frame using a cross-correlation technique. The tracer particles are perceived as a signal and are captured at two instants separated by a known time Δt. The area of interest (AOI) is reflected onto the sensor array of the camera through the imaging optics. To process these signals, each of the two frames of the same image is divided into small, localized subsections, called interrogation windows. The latter are then cross-correlated with each other on a pixel level. This process detects the common linear spatial movement of groups of particles, ΔX, while producing signal peaks that reflect particle locations. The most probable displacements of the particles in each interrogation window can be obtained and thus translated into velocity vectors. Application of cross-correlation to all the interrogation windows over the entire AOI produces a complete two-dimensional Eulerian description of the flow field, which can then be used to obtain various characteristics of the flow of interest such as streamlines, vorticity, circulation, or shear stress. Figure 2.3 displays a clear visualization of the measurement principles of PIV.

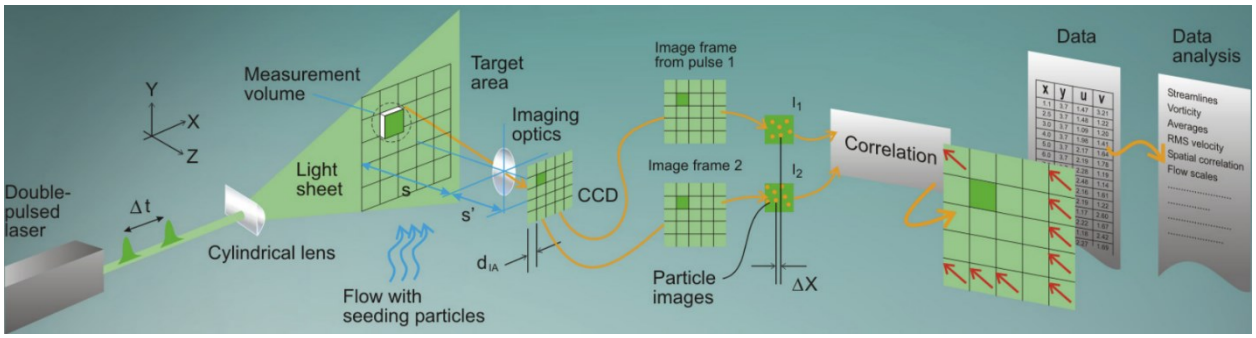

Figure 2.3 Measurement principle of PIV [117]

The time delay Δt between consecutive laser pulses must be small enough to ensure minimal in-plane and out-of-plane loss of particles between the two frames. In practice, it is achieved by ensuring that particle motion within the desired interrogation window size travels no more than a quarter of the distance of the interrogation window [118]–[121]. Preliminary tests suggested that 900 μs was suitable for the different cases studied. Nowadays, interrogation window overlapping and multiple passes of cross-correlation on consecutively smaller interrogation windows allow for overcoming the possible in-plane loss of particle pairs [122], [123].

The fluid used here is water seeded with PSP with a mean particle diameter of 50 μm, with a maximum deviation of ± 20 μm (particles are not perfectly spherical), and a density of 1.03 g/cm^3. The Stokes number is a dimensionless number used to evaluate the response of a particle inertia to viscous drag in a flow. For Stokes numbers above unity, the seed will detach from the flow in the event of an abrupt velocity change, whereas a smaller number ensures that it can follow the streamlines of the flow [124]. This number can be defined as:

$$Stk = \frac{\tau_p}{\tau_f}$$

where the particle relaxation time is given by:

$$\tau_p = \frac{\rho_p d_p^2}{18\mu}$$

ρ_p and d_p are respectively the particle density and diameter, and $\mu = 1.002$ mPa·s is the working fluid dynamic viscosity. The characteristic time scale of the fluid is given by:

$$\tau_f = \frac{L_f}{U_f}$$

where $L_f = 49$ mm is the fluid characteristic length, taken as the minimum piston stroke, and $U_f = 15$ cm/s is the fluid characteristic velocity, corresponding to the jet exit velocity, assumed to be equal to the piston velocity. The Stokes number is found to be $O(10^{-6})$ indicating high responsiveness of the particle to the experimental flow fluctuations.

2.4 Setup calibration and validation

2.4.1 Recording settings

After assembling all the components, the PIV system must be calibrated. To do so, a ruler was positioned facing the camera while aligned with the laser sheet and the center of the pipes. Then, an image is captured to set the mm per pixel scale by defining the distance between two points of the plate displayed on the image. The field of view was adapted to the nozzle spacing and the stroke ratio so that the number of images of the vortex ring displacement recorded was maximized while having the camera close enough to optimize the resolution.

In order to assess the setup performance and find the optimal parameters for the PIV measurements, sets of calibrating experiments with a single jet and double jets were performed. Vibrations of the pipes when the pistons travel were first identified and significantly reduced by fixing the pipes better.

The recording frequency was 200 Hz to maximize the recording time for each experiment, reaching 2.18 s, which corresponds to 436 images. The image definition recorded by the camera is 1632 x 1200 px. As the field of view was adapted to the nozzle spacing, the resolution varied from 179 to 225 points per inch (PPI). This corresponds to a scale factor between 0.14 and 0.11 mm/px, respectively. The interrogation window is 64 x 64 px, and the maximum pixel displacement allowed to be consistent with the condition of one-fourth of the interrogation window size, which is 16 px. This corresponds to 1.76 mm at worse. With a jet exit velocity of 15 cm/s, this gives a

maximum allowable $\Delta t = 1170$ µs. Therefore, the chosen value of 900 µs is suitable. The parameters used for the PIV measurements in the single-jet and double-jet configurations are summarized in Table 2.1. For the sake of brevity, only the parameters for minimum and maximum nozzle spacing, in addition to the single jet configuration, are displayed.

	Single jet	**Double jet** $S/D_0 = 1.49$	**Double jet** $S/D_0 = 3.20$
Seeding particles	PSP, $d_p = 50 \pm 20$ µm, $\rho_p = 1.03$ g/cm^3		
Number of images	436	436	436
Recording frequency (Hz)	200	200	200
Δt (µs)	900	900	900
Recording duration (s)	2.18	2.18	2.18
Image definition (px)	1632 x 1200	1632 x 1200	1632 x 1200
Image resolution (PPI)	225	213	179
Scale factor (mm/px)	0.11	0.12	0.14

Table 2.2 PIV parameters

2.4.2 Processing and post-processing

The resulting vector fields were computed using a multi-pass method, which allows capturing large particle displacements while using small interrogation windows, and no pre-processing. For all the double jet configurations, the multi-pass approach used starts from interrogation windows of 64 x 64 px and ends with interrogation windows of 12 x 12 px. DaVis halves the interrogation window size at each pass until reaching the desired size, hence the two passes used in the first set, corresponding to an initial pass of 64 x 64 px and a second pass of 32 x 32 px. Here, no weighting

function was used. This was followed by three consecutive passes of 16 x 16 px using a round Gaussian weighting function. For all passes, a 50% overlap between interrogation windows was used, therefore improving the final resolution to 8 x 8 px. This method was found to offer the best velocity field resolution with the least number of outliers.

A median filter was also used for outlier detection [125], [126]. It has become a classical method as it is independent of the reference frame and the magnitude of the flow velocities. Indeed, it eliminates a vector based on whether its deviation from the median of its eight neighbors is larger than a standard deviation. Generally, a vector is removed if its deviation falls outside 1 to 3 standard deviations of its neighbors. In this study, the chosen median filter is universal outlier detection (UOD) [127], [128], and one standard deviation was chosen as a criterion. The median filter was applied twice. In the third pass, a reinsertion of good vectors is performed, as long as the vector's deviation from the mean of its neighbors is less than a certain time the standard deviation of its neighbors. Here, the criterion was 3 standard deviations. To fill in data that was removed, a bilinear interpolation was used, in addition to a 3 x 3 denoising technique. In many cases, due to an alignment issue of the two laser pulses, spurious vectors were still present, and that is why a supplementary median filter was applied twice with the same parameters. As some outliers were remaining and the present study focuses on derivative values such as vorticity or swirling strength, it was decided to add a 3 x 3 smoothing.

2.5 Vortex-core identification

Identification of vortices is an interesting tool for understanding complex flow phenomena. However, it can be mathematically hard to implement. The most commonly used methods are based on the velocity gradient tensor, using the Q-criterion, Δ-criterion, λ_2-criterion or swirling strength criterion. Vorticity is not recommended for identification, although it is a suitable method for

visualizing vortices. Other methods have been developed in recent years and are summarized in [129], [130]. For conciseness, they are not described here.

The method used in this study is based on the swirling strength criterion, since it was used in other studies on vortex rings [99] and shows comparable vortex-identification results with the Q-criterion method [131], [132]. This method uses the imaginary part of the complex eigenvalue of ∇u and quantifies the strength of the local swirling motion inside the vortex. Indeed, the velocity gradient tensor in cartesian coordinates can be decomposed as

$$\nabla u = \left[d_{ij}\right] = [\overline{v_r}\,\overline{v_{cr}}\,\overline{v_{ci}}] \begin{bmatrix} \lambda_r & 0 & 0 \\ 0 & \lambda_{cr} & \lambda_{ci} \\ 0 & -\lambda_{ci} & \lambda_{cr} \end{bmatrix} [\overline{v_r}\,\overline{v_{cr}}\,\overline{v_{ci}}]^T$$

where λ_r is the real eigenvalue associated with the eigenvector $\overline{v_r}$ and the complex conjugate pair of complex eigenvalues is $\lambda_{cr} \pm i\lambda_{ci}$ with corresponding eigenvectors $\overline{v_r} \pm i\overline{v_{ci}}$. Let us consider the coordinate system ($\overline{v_r}$, $\overline{v_{cr}}$, $\overline{v_{ci}}$). The local flow is stretched or compressed along the axis $\overline{v_r}$ while it is swirling on the plane spanned by $\overline{v_{cr}}$ and $\overline{v_{ci}}$. Therefore, the strength of this swirling motion is quantified by λ_{ci}. Theoretically, there is a vortex when $\lambda_{ci} > 0$. In practice, it is commonly admitted using $\lambda_{ci} \geq \varepsilon > 0$ as a criterion, where ε was chosen equal to 1.5 in this study, following literature recommendations [132], [133]. This allows for limiting the influence of experimental noise due to the calculation of the velocity gradient tensor from the PIV measurements.

Consistently with [99], the vortex core position can be followed by considering the maximum swirling strength. The clockwise and counterclockwise vortices were distinguished thanks to the sign of the vorticity. A sliding window was also implemented to prevent outlier values and distinguish the different vortex cores. First, this allows the elimination of the images before the

vortex core apparition so that the time scale is the same for all recordings. Secondly, it made the reconnection position identification possible.

2.6 Continuous Wavelet Transform

Although Fourier transforms are commonly used to analyze signals, they capture global frequency information, in other words frequencies that persist over an entire signal. Consequently, local information can be lost in the case of signals with short intervals of characteristic oscillation. Wavelet Transform, which decomposes a function into a set of wavelets, can be a more suitable approach for identifying coherent structures in PIV data [134]. A wavelet is a wave-like oscillation that is localized in time. It is defined by its scale (how stretched it is), and its location (where it is positioned). It follows the convolution principle by computing how much different wavelets are in a signal. The main advantage is that there is a wide range of wavelets that can be chosen to extract local spectral and temporal information simultaneously.

The Morlet wavelet is a complex wavelet commonly used in fluid mechanics as it was demonstrated showing great results for the analysis of fluid properties [135], [136]. The mother function can be described by the following equation:

$$\psi(t) = \pi^{-\frac{1}{4}} e^{-i\omega_0 t} e^{-\frac{t^2}{2}}$$

where ω_0 is the central pulsation of the mother wavelet. The function satisfies $||\psi||^2 = 1$. The Continuous Wavelet Transform (CWT) of a function $x(t)$ at a scale a and translational value b can then be expressed by:

$$X_w(a,b) = \frac{1}{|a|^{\frac{1}{2}}} \int_{-\infty}^{\infty} x(t) \bar{\psi}\left(\frac{t-b}{a}\right) dt$$

A representation of the CWT is displayed in Figure 2.4. The CWT was implemented in MATLAB to perform time-frequency analysis using the `cwt` function.

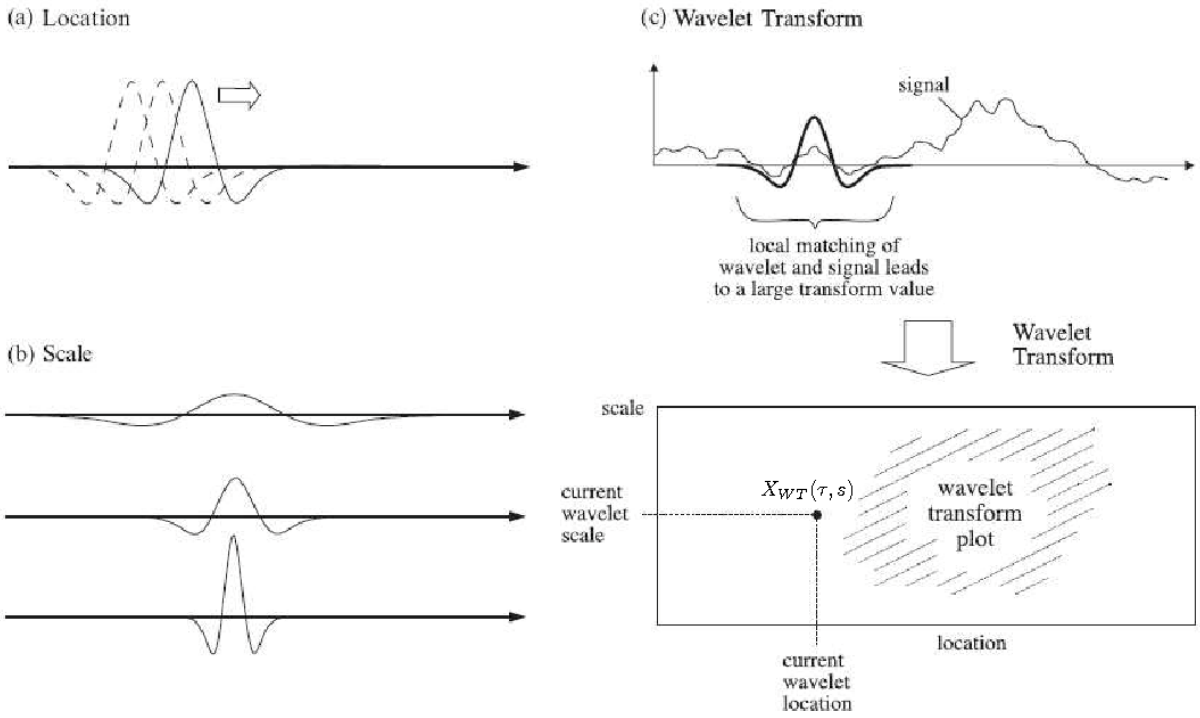

Figure 2.4 Representation of the Continuous Wavelet Transform [137]

3. Results

In this chapter, the results obtained for the different stroke ratios and nozzle spacings are presented. The objective is to see to what extent the distance between the two jet exits and the stroke ratio can influence the vortex ring structure and behavior. First, the results for a single jet will be compared to the literature. Then, the vorticity contours and velocity fields at different time instants are displayed. In addition to this, the vortex core positions are followed to identify the reconnection points and eventually perform time-frequency analysis thanks to CWT.

In the rest of this chapter, spatial coordinates are normalized by the cylinder diameter D_0. Time and vorticity are normalized by D_0 and the piston velocity U_p so that it corresponds to the formation time $T = t * U_p/D_0$ and $\omega^* = \omega * D_0/U_p$, respectively.

3.1 Single vortex ring configuration

The objective of this section is to validate the results for a single jet configuration. To do so, the average streamwise position of the vortex cores in function of the formation time is plotted in Figure 3.1, using the swirling strength criterion.

As highlighted in [90], after a certain time, the forming vortex ring reaches a steady translating velocity, characterized by a linear evolution of the streamwise position. The related normalized translating velocity U_{tr}/U_p corresponds to the slope of the line, as estimated in Figure 3.1 (b). It is worth noting that this velocity increases with the stroke ratio, which is consistent with the literature [87], [90], [96]. The obtained translating velocity is compared with the results of Mohseni and Gharib [96] in Table 3.1. Since they focused only on U_{tr} varying from $0.5U_p$ to $0.6U_p$, the value obtained for $L/D_0 = 2$ can not be compared. Nevertheless, the other values measured in this study are highly consistent with their results since the difference is low. It is also interesting to note that

the translating velocity is around half the piston velocity, which is what the slug model predicts [96].

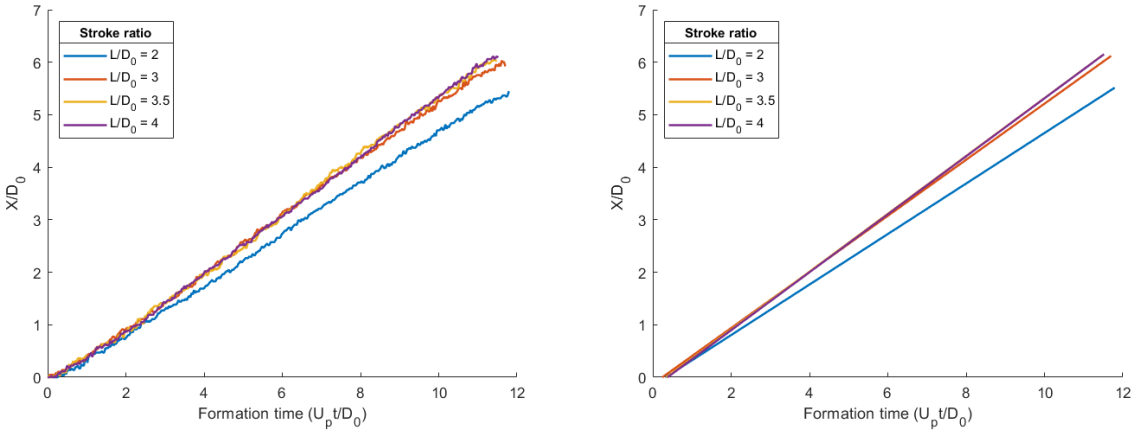

Figure 3.1 Average streamwise position of the vortex cores as a function of formation time for stroke ratios of 2, 3, 3.5 and 4: (a) raw data and (b) linear estimation

L/D_0	U_{tr}/U_p measured	U_{tr}/U_p in [96]	Difference
2	0.481	X	X
3	0.534	0.505	5.8%
3.5	0.550	0.525	4.9%
4	0.552	0.575	4.0%

Table 3.1 Comparison of normalized translating velocity of the vortex cores with the results of Mohseni and Gharib [96]

3.2 Flow visualization

The velocity fields and vorticity contours for different time instants have been analyzed for all cases. The results for nozzle spacings of 1.49, 2.19 and 3.20 can be found in Figure 3.2. A more detailed view can be found for a stroke ratio of 2 in Figure 3.3. The results for the other cases can

be found in the Appendix. As it is a two-dimensional visualization, what is observed here is a cross-section of the vortex rings. Therefore, two vortex cores can be identified for each vortex ring. Although they correspond to the same structure, in the following, the vortex cores which are closer to the other vortex ring will be called "internal", whereas the extreme vortex cores will be called "external", as shown in Figure 3.3.

In the interaction zone, the streamwise velocity decreases, leading to a gap between the streamwise positions of the reconnecting vortices and the external vortices, which are not affected by the interaction yet. Once merged, the external cores of the newly formed vortex ring get closer until a critical distance, before getting away from each other again. It can also be noticed that the area of the vortex cores and the vorticity significantly decrease. This is consistent with the sinusoidal instability observed in the literature [109], [113]. Indeed, during the reconnection, the interaction zone is bent in the direction perpendicular to the view section. Thus, the velocity field in the reconnection zone becomes a complex three-dimensional structure.

To further investigate the drop in vorticity, its evolution was plotted for each vortex core, as in Figure 3.4. Only the case $S/D_0 = 2.45$ with a stroke ratio of 2 is displayed for conciseness matter. As long as the vortex rings do not interact, the vorticity of the internal cores equals the vorticity of the external cores. When the vortex rings start interacting, the vorticity of the internal cores collapses to reach null vorticity, which corresponds to the moment when they are fully merged and start stretching to form one unique vortex ring, as schematized in Figure 3.4. Only the results for $S/D_0 = 3.20$ are different since there is no vortex ring interaction. The observations are similar for all other cases, except the instant when the vorticity drop occurs which obviously happens earlier as the nozzle spacing decreases.

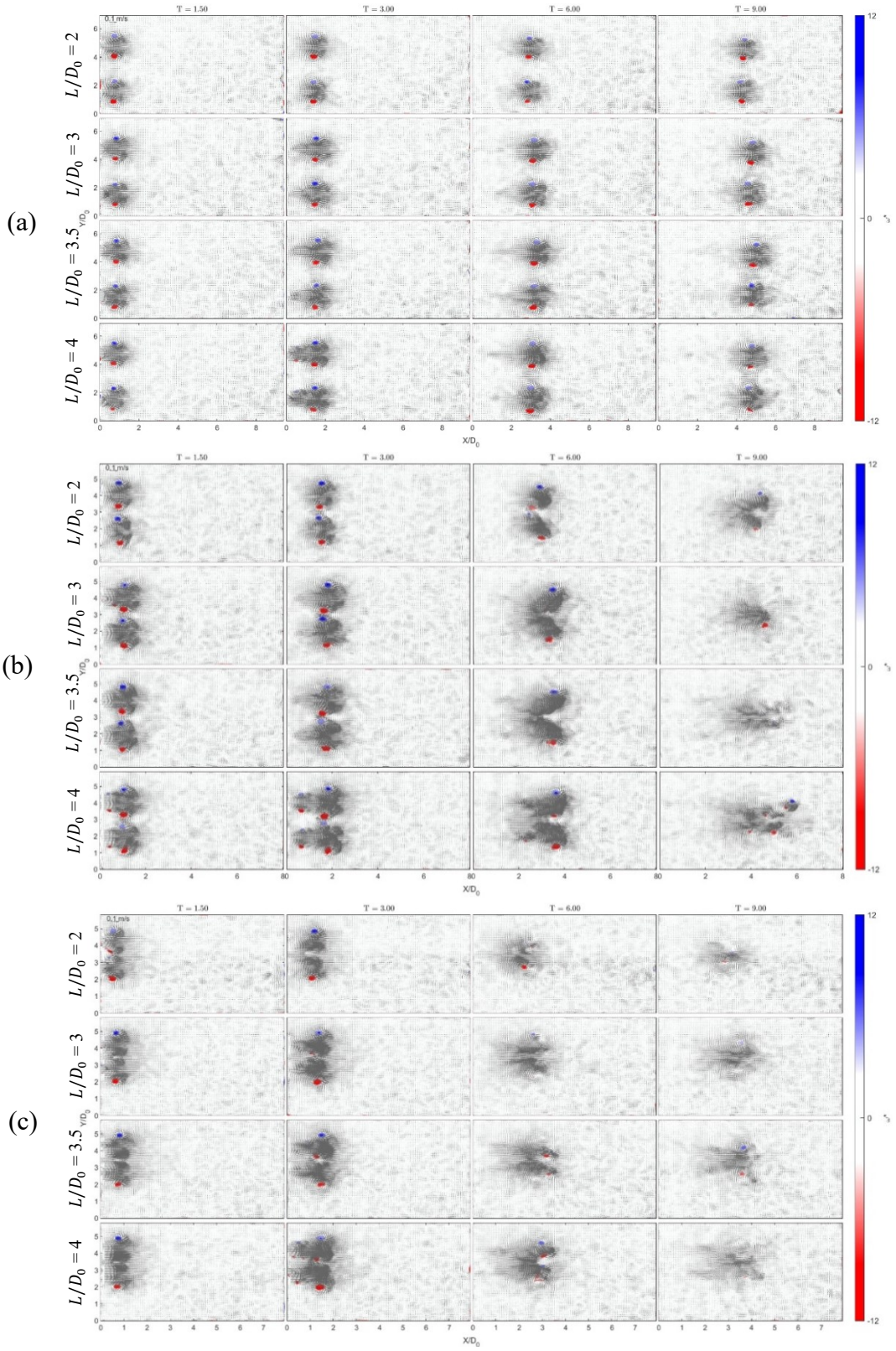

Figure 3.2 Velocity fields and vorticity contours at different time instants and stroke ratio for a nozzle spacing (a) $S/D_0 = 3.20$; (b) $S/D_0 = 2.19$; (c) $S/D_0 = 1.49$

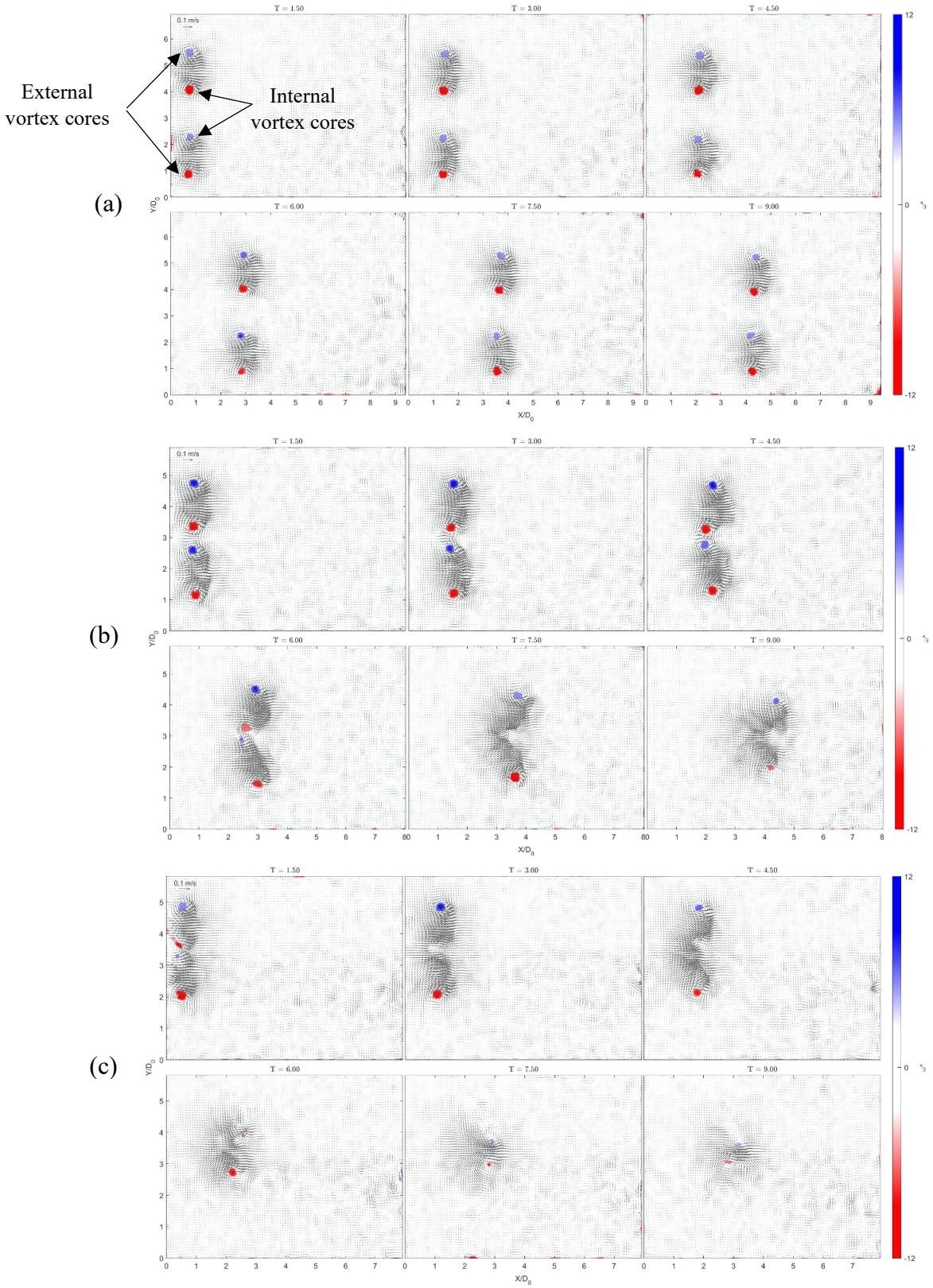

Figure 3.3 Velocity fields and vorticity contours at different time instants for a stroke ratio of $L/D_0 = 2$ and a nozzle spacing of (a) $S/D_0 = 3.20$; (b) $S/D_0 = 2.19$; (c) $S/D_0 = 1.49$

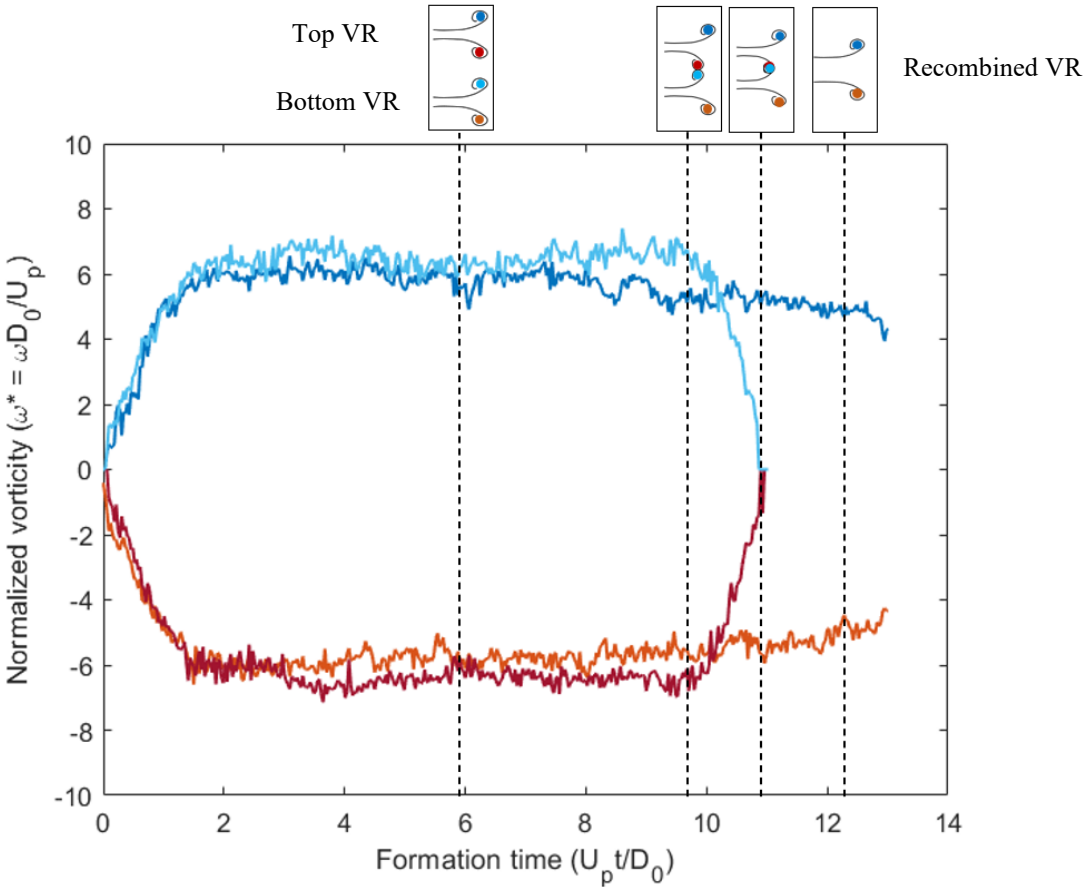

Figure 3.4 Vorticity of the vortex cores for a nozzle spacing $S/D_0 = 2.45$ and a stroke ratio $L/D_0 = 2$ ('VR' stands for vortex ring)

3.3 Reconnection localization

The previous results suggest that there is a critical nozzle spacing from which the two vortex rings attract each other. Above this value, they simply evolve as two parallel single-pulsed jets. Figure 3.5 summarizes whether reconnection was observed for the different cases. The reconnection phenomenon appears to depend more on the nozzle spacing than on the stroke ratio. In the case $S/D_0 = 3.20$, the two cylinders were too far, thus no interaction was observed. This suggests a critical spacing ratio of around 3, a value above which vortex rings do not interact. This is consistent with the observations of Athanassiadis and Hart [6]. For $S/D_0 = 1.49$, they were so

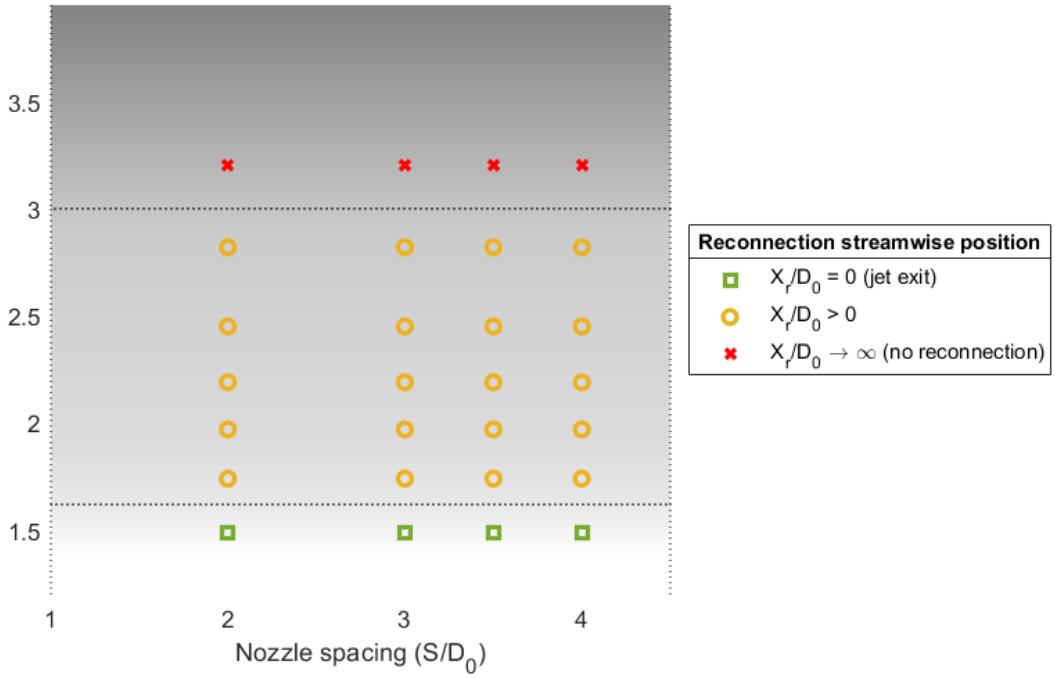

Figure 3.5 Reconnection of the vortex rings depending on nozzle spacing S/D_0 and stroke ratio L/D_0

close that the internal vortex cores already merged at the jet exit. In the other cases, the vortex rings first attract each other and then merge once they are close enough.

It can also be noticed that, following the nozzle spacing, they will not merge at the same streamwise position. To further investigate this, each vortex core was identified, and their position followed. To do so, the swirling strength vortex identification approach was combined with a sliding window method to distinguish the external and internal vortices, as well as the clockwise and counterclockwise vortices. The position where the two internal vortices can not be distinguished anymore corresponds to the last location where the swirling strength was superior to 1.5. This position is called the reconnection point and its streamwise position will be written X_r in the following. The results for each case can be found in Figure 3.6. Unfortunately, for $S/D_0 = 2.82$, the recording time was not long enough to localize the reconnection points for stroke ratios

of 2, 3 and 3.5, although it can still be asserted that the vortex rings merged. Therefore, only the result for $L/D_0 = 4$ is presented for this nozzle spacing value.

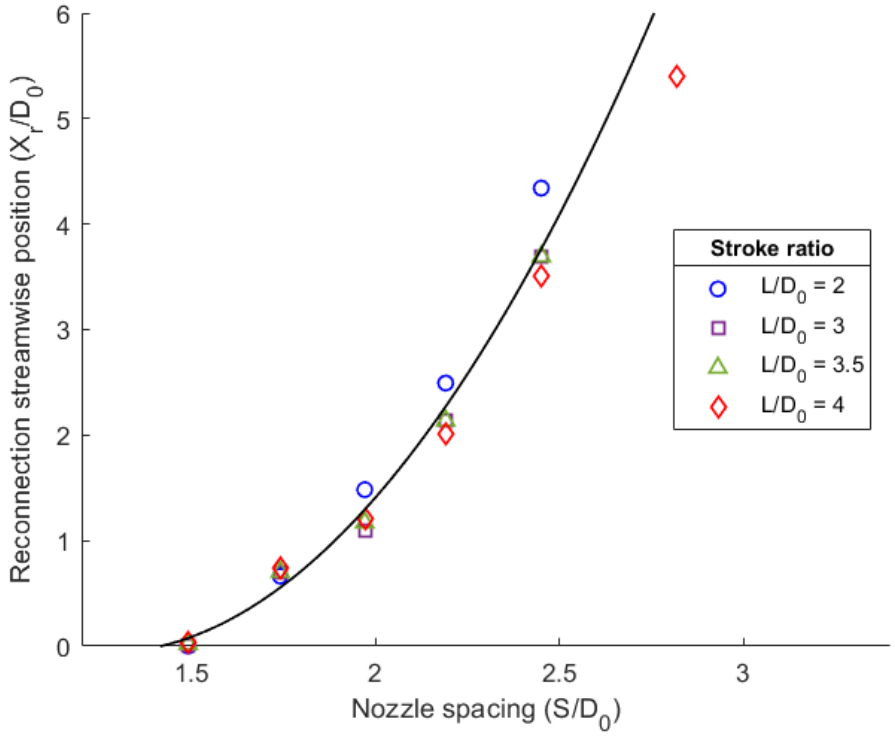

Figure 3.6 Reconnection position as a function of nozzle spacing S/D_0 for different stroke ratios

The evolution of X_r/D_0 in function of S/D_0 can be described by a second-order polynomial with a coefficient of 2.72, corresponding to the black line on the graph in Figure 3.6. It is interesting to notice that the most impactful parameter is nozzle spacing. However, it can be observed that the influence of the stroke ratio increases with the nozzle spacing. Indeed, for $S/D_0 \geq 1.74$, the vortex rings merge further as the stroke ratio decreases, and this gap between the lower and higher values of L/D_0 becomes more significant as the distance between the nozzle exits increases.

3.4 Time-frequency analysis

Since the reconnection points of the two vortex rings have been localized, it can be interesting to focus on what is happening during the interaction. For this purpose, we used complex Morlet

wavelet transform to investigate turbulence in the flow at the reconnection point, as well as before and after. Consequently, time-frequency analysis of the velocity is performed at three localizations, except for $S/D_0 = 3.20$ and $S/D_0 = 1.49$, as explained below. The results were found very similar for the u-component and v-component. Thus, only the first one will be discussed in this investigation.

For $S/D_0 = 3.20$, since no reconnection is observed, the time-frequency spectra are displayed in Figure 3.7 for a signal obtained in the middle between the two vortex rings and at an arbitrary streamwise position. Due to its similarity with the other stroke ratios, only the case $L/D_0 = 2$ is displayed here. As expected, no significant frequency variation is observed since there was no interaction between the two vortex rings. The spectra were very similar for different streamwise positions.

The following figures display the time-frequency spectra for all cases. A schematic was added to illustrate the phase when the signal is extracted. The red cross corresponds to the point where the signal was obtained (before the reconnection, at the reconnection point and after the

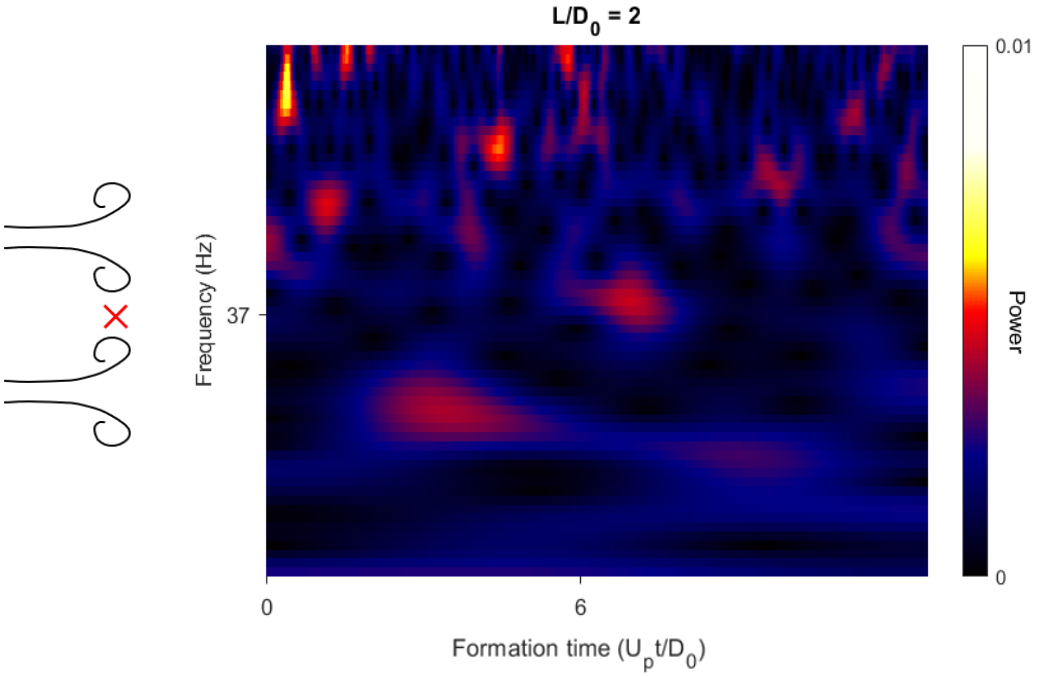

Figure 3.7 Time-frequency spectra of the u-component velocity for $S/D_0 = 3.20$ and $L/D_0 = 2$

reconnection). In all results, the flow before and after reconnection is characterized by low-frequency variations. At the reconnection point, it is particularly interesting to notice a high-frequency peak during a short period. This is the signature of highly fast changes in the flow behavior. This can be associated with high spatial fluctuation of energy and a stronger turbulence intensity. Since wavelets are a spatial indicator of signal variations, this is consistent with the velocity changes observed previously. This peak is not present before reconnecting since the structure of the vortex rings is not affected yet. It is not visible after reconnection either, which means the bending of the internal vortices in the direction perpendicular to the section defined by the center of the nozzle exits is finished. Moreover, it is coherent to observe that the closer the jets are, the sooner this peak is observed.

In the case $S/D_0 = 1.49$, only two points were placed since the vortex rings are already interacting at the nozzle exit. As expected, the high-frequency peak is already observed at this location, which confirms that the jets are so close that reconnection is already happening at the jet exit. For $S/D_0 = 2.82$, where the reconnection point could only be localized for $L/D_0 = 4$ due to recording time limitation, the same locations were used for all stroke ratio values, based on the case

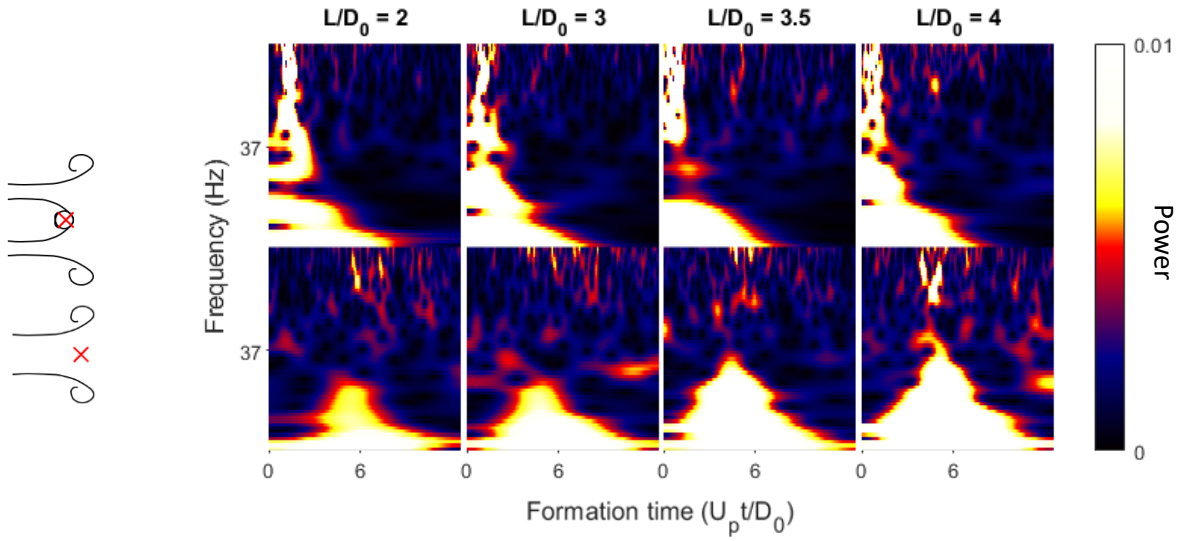

Figure 3.8 Time-frequency spectra of the u-component velocity for $S/D_0 = 1.49$

with a stroke ratio of 4. The high-frequency peak is therefore observed for this case and starts to be visible for $L/D_0 = 3.5$, just before the end of the recording. For the other stroke ratios, it is indeed not observed.

In addition, the greater the nozzle spacing, the later the high-frequency variations are observed, which is consistent with the results in Figure 3.6. Moreover, for $S/D_0 \geq 1.97$, the high-frequency variations are observed slightly later as the stroke ratio decreases. It confirms that the most influencing parameter is nozzle spacing. Nevertheless, no major discrepancy was observed in power nor time duration between the different stroke ratios or nozzle spacings.

These results are consistent with [15], who also observed a high-frequency peak as the vortex ring goes by the signal extraction point. However, they did not mention any discrepancy between different streamwise positions for an extraction point placed in the middle of the two vortex rings. This might be because their investigation corresponds to a nozzle spacing close to 1, which might not allow observing a vortex ring reconnection due to a too strong turbulence at the jet exit. As a matter of fact, they did not report reconnection observation in the case of a sutured mitral valve model.

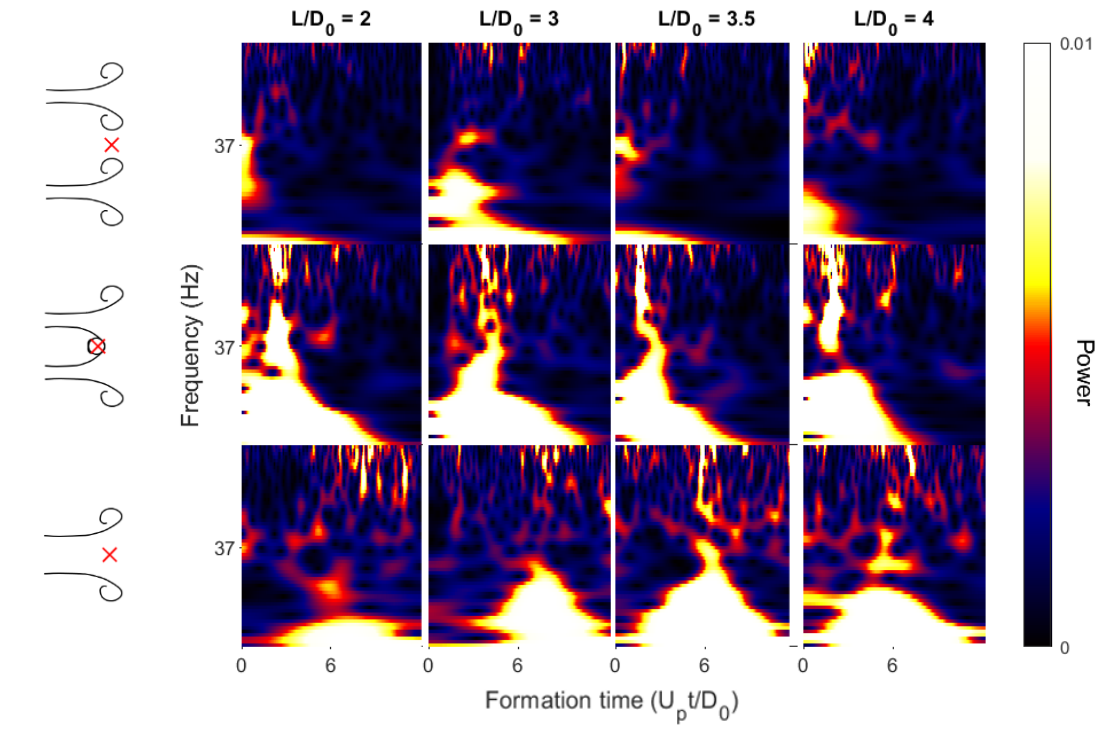

Figure 3.9 Time-frequency spectra of the u-component velocity for $S/D_0 = 1.74$

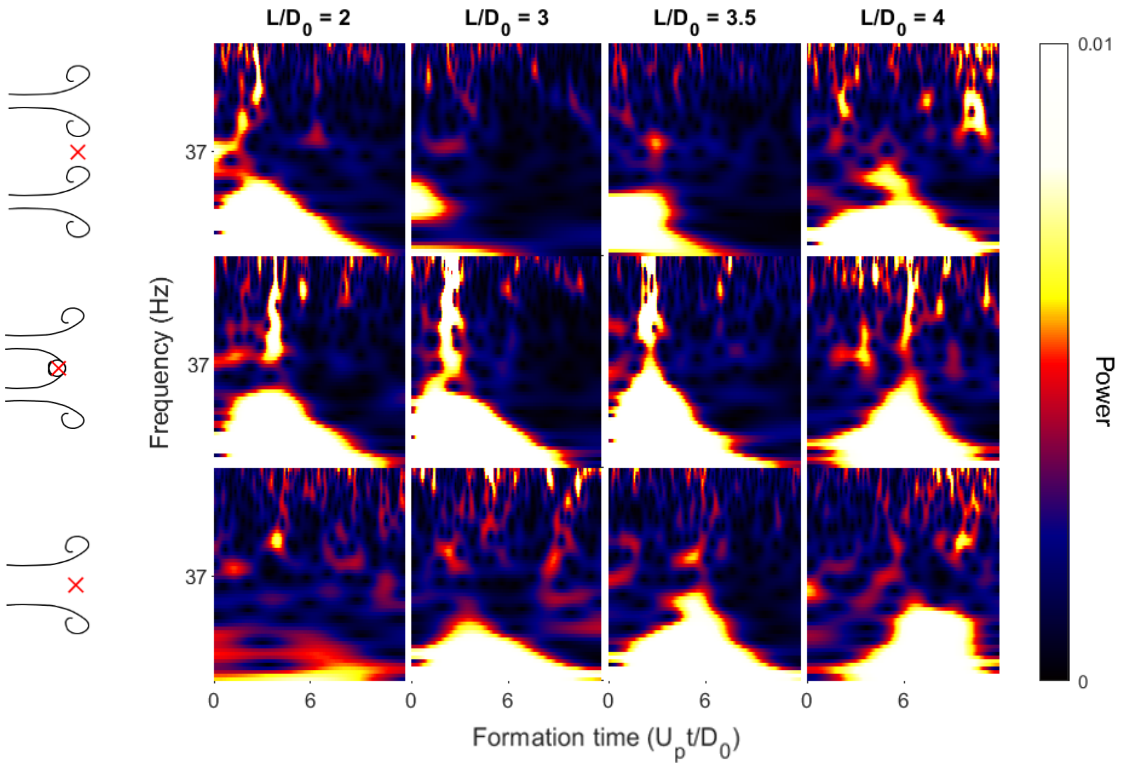

Figure 3.10 Time-frequency spectra of the u-component velocity for $S/D_0 = 1.97$

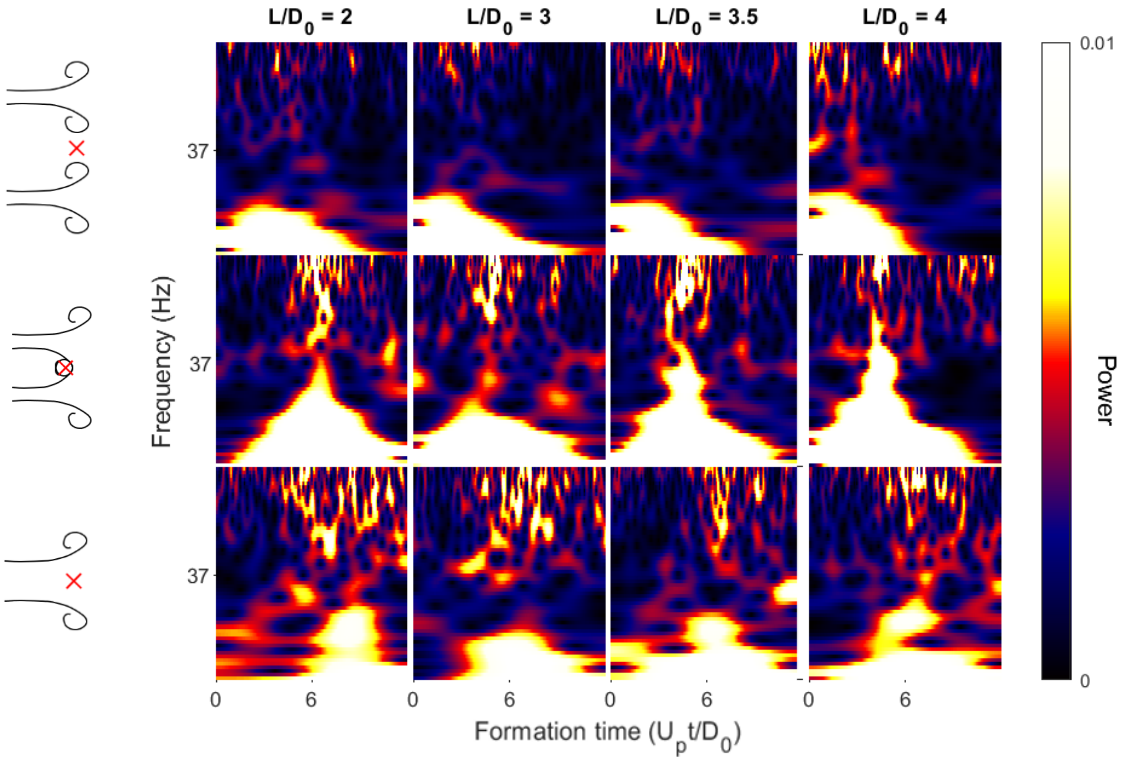

Figure 3.11 Time-frequency spectra of the u-component velocity for $S/D_0 = 2.19$

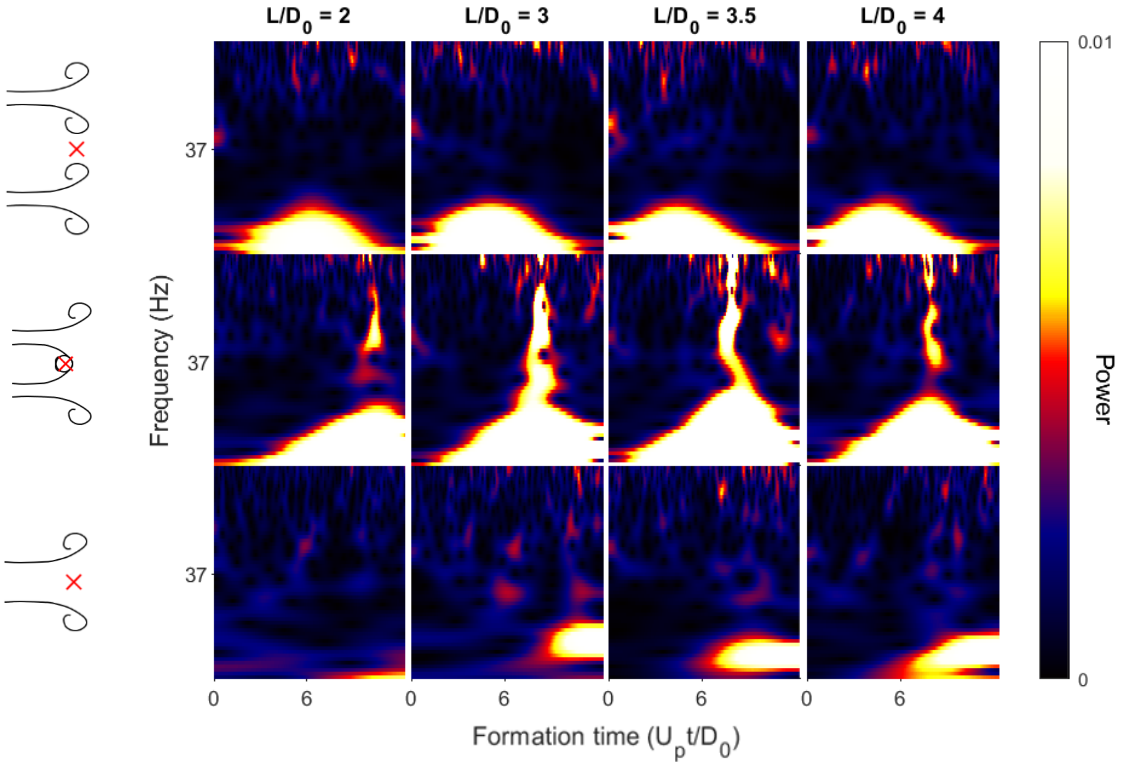

Figure 3.10 Time-frequency spectra of the u-component velocity for $S/D_0 = 2.45$

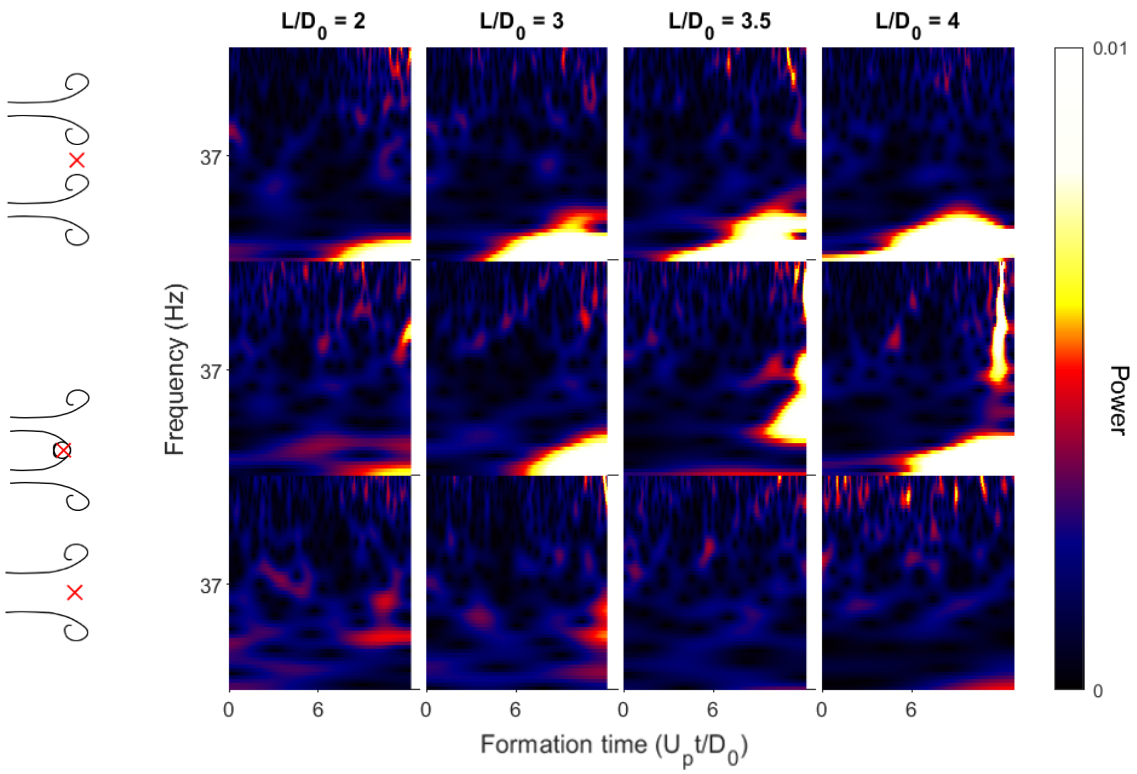

Figure 3.11 Time-frequency spectra of the u-component velocity for $S/D_0 = 2.82$

4. Conclusion and future work

Although pulsed jets have been investigated for decades, the reconnection of twin parallel vortex rings remains rarely studied. In the present investigation, an experimental setup has been developed to observe this reconnection for several nozzle spacings, but also different stroke ratios. The PIV measurements allowed the flow fields and vorticity contours during this phenomenon to be visualized. By identifying the vortex core location, it became possible to localize the reconnection points and unveil the influence of the nozzle spacing and the stroke ratio. Finally, a time-frequency analysis was performed at the reconnection point, but also before and after, in order to better describe the complexity of the structure changes when reconnecting.

All in all, the results confirm how important the reconnection is in the stability of the structure. Indeed, when vortex rings merge, highly fast changes in velocity are observed, suggesting it is a turning point in the structure of the vortex rings. This is confirmed by the drop in vorticity observed when they start interacting. Indeed, when the two vortex rings reconnect, their structure is not stable anymore. Therefore, they will try to adapt as fast as possible so that they can reach a new stable structure, which is a circle, or in other words, a single vortex ring.

It is also important to discuss the influence of the nozzle spacing and the stroke ratio. First, a critical spacing ratio of around 3 was identified. Indeed, above this value, no vortex ring interaction was observed. Below 1.5, the results showed the vortex rings are already merged at the jet exit. The results also suggest that the most influential parameter is the nozzle spacing, especially for $S/D_0 < 2$. However, above this value, the influence of the stroke ratio becomes more important. As a result, when L/D_0 decreases, the reconnection point position increases. This can be explained by a lower circulation for smaller stroke ratios [90], entailing a slower vortex reconnection.

Furthermore, a greater number of experiment repetitions could improve the results, more particularly the reconnection point values. For further work, it could be interesting to increase the number of nozzle spacings, with a focus on the critical value from which the vortex rings start interacting. It can also be interesting to investigate the influence of a trailing jet by generating strokes with a ratio $L/D_0 > 4$. Moreover, the use of Tomographic PIV would be very beneficial for a volumetric description of the vortex structure after reconnection. Indeed, when the vortex rings start interacting, a stretching occurs, bending the interaction zone in the direction perpendicular to the section studied here. Therefore, Tomographic PIV would allow for further scrutinizing the velocity and vorticity changes from the reconnection point. Finally, it would be worth investigating the influence of other parameters, such as viscosity, the geometry of the nozzle exit, a time delay between the two strokes, a difference between the two cylinder diameters, an angle between the two jets, or the presence of boundaries. More specifically, particular attention should be paid to the physics of twin pulsed jets within an elastic cavity. This would lead to a better understanding of the interaction between vortex rings in the cardiac mechanism.

Bibliography

[1] J. Mi, G. J. Nathan, and D. S. Nobes, "Mixing characteristics of axisymmetric free jets from a contoured nozzle, an orifice plate and a pipe," *Journal of Fluids Engineering*, vol. 123, no. 4, pp. 878–883, Jun. 2001, doi: https://doi.org/10.1115/1.1412460.

[2] P. E. Dimotakis, "The mixing transition in turbulent flows," *Journal of Fluid Mechanics*, vol. 409, pp. 69–98, Apr. 2000, doi: https://doi.org/10.1017/s0022112099007946.

[3] Z. Yin, H. Zhang, and J. Lin, "Experimental study on the flow field characteristics in the mixing region of twin jets," *Journal of Hydrodynamics*, vol. 19, no. 3, pp. 309–313, Jun. 2007, doi: https://doi.org/10.1016/s1001-6058(07)60063-8.

[4] A. Durve, A. W. Patwardhan, I. Banarjee, G. Padmakumar, and G. Vaidyanathan, "Numerical investigation of mixing in parallel jets," *Nuclear Engineering and Design*, vol. 242, pp. 78–90, Jan. 2012, doi: https://doi.org/10.1016/j.nucengdes.2011.10.051.

[5] I. Zawadzki and H. Aref, "Mixing during vortex ring collision," *Physics of Fluids A: Fluid Dynamics*, vol. 3, no. 5, pp. 1405–1410, May 1991, doi: https://doi.org/10.1063/1.858204.

[6] A. G. Athanassiadis and D. P. Hart, "Effects of multijet coupling on propulsive performance in underwater pulsed jets," *Physical Review Fluids*, vol. 1, no. 3, Jul. 2016, doi: https://doi.org/10.1103/physrevfluids.1.034501.

[7] K. Knowles and A. J. Saddington, "A review of jet mixing enhancement for aircraft propulsion applications," *Journal of Aerospace Engineering*, vol. 220, no. 2, pp. 103–127, Feb. 2006, doi: https://doi.org/10.1243/09544100g01605.

[8] Y. Luo, Q. Xiao, Q. Zhu, and G. Pan, "Pulsed-jet propulsion of a squid-inspired swimmer at high Reynolds number," *Physics of Fluids*, vol. 32, no. 11, p. 111901, Nov. 2020, doi: https://doi.org/10.1063/5.0027992.

[9] I. K. Bartol, P. S. Krueger, W. J. Stewart, and J. T. Thompson, "Pulsed jet dynamics of squid hatchlings at intermediate Reynolds numbers," *Journal of Experimental Biology*, vol. 212, no. 10, pp. 1506–1518, May 2009, doi: https://doi.org/10.1242/jeb.026948.

[10] A. Kheradvar and M. Gharib, "On mitral valve dynamics and its connection to early diastolic flow," *Annals of Biomedical Engineering*, vol. 37, no. 1, pp. 1–13, Nov. 2008, doi: https://doi.org/10.1007/s10439-008-9588-7.

[11] A. El Sabbagh, Y. N. V. Reddy, and R. A. Nishimura, "Mitral valve regurgitation in the contemporary era," *JACC: Cardiovascular Imaging*, vol. 11, no. 4, pp. 628–643, Apr. 2018, doi: https://doi.org/10.1016/j.jcmg.2018.01.009.

[12] O. Smadi, I. Hassan, P. Pibarot, and L. Kadem, "Numerical and experimental investigations of pulsatile blood flow pattern through a dysfunctional mechanical heart valve," *Journal of Biomechanics*, vol. 43, no. 8, pp. 1565–1572, May 2010, doi: https://doi.org/10.1016/j.jbiomech.2010.01.029.

[13] M. Gharib, E. Rambod, A. Kheradvar, D. J. Sahn, and J. O. Dabiri, "Optimal vortex formation as an index of cardiac health," *Proceedings of the National Academy of Sciences*, vol. 103, no. 16, pp. 6305–6308, Apr. 2006, doi: https://doi.org/10.1073/pnas.0600520103.

[14] G. Di Labbio and L. Kadem, "Jet collisions and vortex reversal in the human left ventricle," *Journal of Biomechanics*, vol. 78, pp. 155–160, Sep. 2018, doi: https://doi.org/10.1016/j.jbiomech.2018.07.023.

[15] M. Sargordi, A. Chtchetinina, G. Di Labbio, H. D. Ng, and L. Kadem, "Pulsatile twin parallel jets through a flexible orifice with application to edge-to-edge mitral valve repair," *Physics of Fluids*, vol. 32, no. 12, pp. 121702–121702, Dec. 2020, doi: https://doi.org/10.1063/5.0025859.

[16] M. Qintar and A. K. Chhatriwalla, "Update on the current status and indications for

transcatheter edge-to-edge mitral valve repair," *Current Cardiology Reports*, vol. 22, no. 11, Sep. 2020, doi: https://doi.org/10.1007/s11886-020-01391-1.

[17] A. Chtchetinina, *Experimental Investigation of Jets Through a Model Mitral Valve with Different Leaflet Suture Configurations*, Master Thesis, Concordia University, Montréal, Canada, 2015.

[18] M. Sargordi, *Flow Characteristics Downstream of Twin Pulsed Orifice Jets: Application to Mitral Valve Repair*, Master Thesis, Concordia University, Montréal, Canada, 2020.

[19] K. Mohseni, "Pulsatile vortex generators for low-speed maneuvering of small underwater vehicles," *Ocean Engineering*, vol. 33, no. 16, pp. 2209–2223, Nov. 2006, doi: https://doi.org/10.1016/j.oceaneng.2005.10.022.

[20] L. P. Madin, "Aspects of jet propulsion in salps," *Canadian Journal of Zoology*, vol. 68, no. 4, pp. 765–777, Apr. 1990, doi: https://doi.org/10.1139/z90-111.

[21] Q. Bone and E. R. Trueman, "Jet propulsion in salps (Tunicata: Thaliacea)," *Journal of Zoology*, vol. 201, no. 4, pp. 481–506, Dec. 1983, doi: https://doi.org/10.1111/j.1469-7998.1983.tb05071.x.

[22] J. H. Costello, S. P. Colin, B. J. Gemmell, J. O. Dabiri, and K. R. Sutherland, "Multi-jet propulsion organized by clonal development in a colonial siphonophore," *Nature Communications*, vol. 6, no. 1, p. 8158, Sep. 2015, doi: https://doi.org/10.1038/ncomms9158.

[23] "Siphonophorae," *Wikipedia*, Apr. 07, 2023. https://fr.wikipedia.org/w/index.php?title=Siphonophorae&oldid=203040108 (accessed Jun. 02, 2023).

[24] M. I. Gurevich, *The Theory of Jets in Ideal Fluids*. Elsevier, 1965.

[25] Sergeĭ Alekseevich Chaplygin, *Gas Jets*. National Advisory Committee for Aeronautics, 1944.

[26] M. Kaushik, R. Kumar, and Humrutha G, "Review of computational fluid dynamics studies

on jets," *American Journal of Fluid Dynamics*, vol. 5, no. 3A, pp. 1–11, Jan. 2015.

[27] G. N. Abramovich, "General properties of turbulent jets," in *The Theory of Turbulent Jets*, MIT Press, 1963, pp. 3–49.

[28] C. D. Richards and W. M. Pitts, "Global density effects on the self-preservation behaviour of turbulent free jets," *Journal of Fluid Mechanics*, vol. 254, pp. 417–435, Sep. 1993, doi: https://doi.org/10.1017/s0022112093002204.

[29] G. F. Xu and R. A. Antonia, "Effect of different initial conditions on a turbulent round free jet," *Experiments in Fluids*, vol. 33, no. 5, pp. 677–683, Nov. 2002, doi: https://doi.org/10.1007/s00348-002-0523-7.

[30] V. Todde, P. G. Spazzini, and M. Sandberg, "Experimental analysis of low-Reynolds number free jets," *Experiments in Fluids*, vol. 47, no. 2, pp. 279–294, Apr. 2009, doi: https://doi.org/10.1007/s00348-009-0655-0.

[31] S. C. Crow and F. H. Champagne, "Orderly structure in jet turbulence," *Journal of Fluid Mechanics*, vol. 48, no. 3, pp. 547–591, Aug. 1971, doi: https://doi.org/10.1017/S0022112071001745.

[32] S. J. Kwon and I. W. Seo, "Reynolds number effects on the behavior of a non-buoyant round jet," *Experiments in Fluids*, vol. 38, no. 6, pp. 801–812, Apr. 2005, doi: https://doi.org/10.1007/s00348-005-0976-6.

[33] A. Abdel-Rahman, "A review of effects of initial and boundary conditions on turbulent jets," *WSEAS transactions on Fluid Mechanics*, vol. 4, no. 5, pp. 257–275, 2010.

[34] N. Georgiadis and D. Papamoschou, "Computational investigations of high speed dual stream jets," in *9th AIAA/CEAS Aeronautics Conference and Exhibit*, Hilton Head, SC, May 2003, p. 3311.

[35] N. Rajaratnam and K. Subramanya, "Plane turbulent reattached wall jets," *Journal of the*

Hydraulics Division, vol. 94, no. 1, pp. 95–112, Jan. 1968, doi: https://doi.org/10.1061/jyceaj.0001771.

[36] J. Hoch and L. M. Jiji, "Two-dimensional turbulent offset jet-boundary interaction," *Journal of Fluids Engineering*, vol. 103, no. 1, pp. 154–161, Mar. 1981, doi: https://doi.org/10.1115/1.3240766.

[37] C. Bourque and B. G. Newman, "Reattachment of a two-dimensional, incompressible jet to an adjacent flat plate," *The Aeronautical Quarterly*, vol. 11, no. 3, pp. 201–232, Aug. 1960, doi: https://doi.org/10.1017/s0001925900001797.

[38] R. Pelfrey and J. A. Liburdy, "Mean flow characteristics of a turbulent offset jet," *Journal of Fluids Engineering*, vol. 108, no. 1, pp. 82–88, Mar. 1986, doi: https://doi.org/10.1115/1.3242548.

[39] M. Agelin-Chaab and M. F. Tachie, "Characteristics of turbulent three-dimensional offset jets," *Journal of Fluids Engineering*, vol. 133, no. 5, pp. 608-620, May 2011, doi: https://doi.org/10.1115/1.4004071.

[40] A. Assoudi, S. Habli, N. M. Saïd, H. Bournot, and G. Le Palec, "Experimental and numerical study of an offset jet with different velocity and offset ratios," *Engineering Applications of Computational Fluid Mechanics*, vol. 9, no. 1, pp. 490–512, Jan. 2015, doi: https://doi.org/10.1080/19942060.2015.1071525.

[41] A. Assoudi, A. Amamou, N. M. Saïd, and H. Bournot, "Characteristics and analysis of a turbulent offset jet including the effect of density and offset height," *International Journal of Mechanical Sciences*, vol. 174, pp. 105477–105477, May 2020, doi: https://doi.org/10.1016/j.ijmecsci.2020.105477.

[42] V. Parameswaran and S. A. Alpay, "Studies on re-attaching wall jets," *Transactions of the Canadian Society for Mechanical Engineering*, vol. 3, no. 2, pp. 83–89, Jun. 1975, doi:

https://doi.org/10.1139/tcsme-1975-0012.

[43] A. Nasr and J. C. S. Lai, "A turbulent plane offset jet with small offset ratio," *Experiments in Fluids*, vol. 24, no. 1, pp. 47–57, Jan. 1998, doi: https://doi.org/10.1007/s003480050149.

[44] B. E. Launder and W. Rodi, "The turbulent wall jet measurements and modeling," *Annual Review of Fluid Mechanics*, vol. 15, no. 1, pp. 429–459, Jan. 1983, doi: https://doi.org/10.1146/annurev.fl.15.010183.002241.

[45] A. Dejoan and M. A. Leschziner, "Large eddy simulation of a plane turbulent wall jet," *Physics of Fluids*, vol. 17, no. 2, p. 025102, Feb. 2005, doi: https://doi.org/10.1063/1.1833413.

[46] W. K. George, H. Abrahamsson, J. Eriksson, R. I. Karlsson, L. Löfdahl, and M. Wosnik, "A similarity theory for the turbulent plane wall jet without external stream," *Journal of Fluid Mechanics*, vol. 425, pp. 367–411, Dec. 2000, doi: https://doi.org/10.1017/s002211200000224x.

[47] J. G. Eriksson, R. I. Karlsson, and J. L. Persson, "An experimental study of a two-dimensional plane turbulent wall jet," *Experiments in Fluids*, vol. 25, no. 1, pp. 50–60, Jun. 1998, doi: https://doi.org/10.1007/s003480050207.

[48] K. Zhou and Herlina, "An experimental study on turbulent circular wall jets," *Journal of Hydraulic Engineering*, vol. 128, no. 2, pp. 161–174, Feb. 2002, doi: https://doi.org/10.1061/(asce)0733-9429(2002)128:2(161).

[49] H. A. Hussein, S. P. Capp, and W. H. George, "Velocity measurements in a high-Reynolds-number, momentum-conserving, axisymmetric, turbulent jet," *Journal of Fluid Mechanics*, vol. 258, pp. 31–75, Jan. 1994, doi: https://doi.org/10.1017/s002211209400323x.

[50] W. K. George, R. E. A. Arndt, and S. Corrsin, *Advances in Turbulence*. New York City: Hemisphere Pub. Corp, 1989.

[51] I. Wygnanski and H. Fiedler, "Some measurements in the self-preserving jet," *Journal of Fluid*

Mechanics, vol. 38, no. 3, pp. 577–612, Sep. 1969, doi: https://doi.org/10.1017/s0022112069000358.

[52] A. Agrawal and A. S. Prasad, "Properties of vortices in the self-similar turbulent jet," *Experiments in Fluids*, vol. 33, no. 4, pp. 565–577, Oct. 2002, doi: https://doi.org/10.1007/s00348-002-0507-7.

[53] P. Burattini, R. A. Antonia, and S. Rajagopalan, "Effect of initial conditions on the far field of a round jet," in *15th Australasian Fluid Mechanics Conference*, Sydney, NSW, Australia, 2004.

[54] D. R. Dowling and P. E. Dimotakis, "Similarity of the concentration field of gas-phase turbulent jets," *Journal of Fluid Mechanics*, vol. 218, no. -1, p. 109, Sep. 1990, doi: https://doi.org/10.1017/s0022112090000945.

[55] B. Liu, J. Mi, and G. J. Nathan, "The influence of nozzle aspect ratio on plane jets," *Experimental Thermal and Fluid Science*, vol. 31, no. 8, pp. 825–838, Aug. 2007, doi: https://doi.org/10.1016/j.expthermflusci.2006.08.009.

[56] W. R. Quinn, "Experimental study of the near field and transition region of a free jet issuing from a sharp-edged elliptic orifice plate," *European Journal of Mechanics - B/Fluids*, vol. 26, no. 4, pp. 583–614, Jul. 2007, doi: https://doi.org/10.1016/j.euromechflu.2006.10.005.

[57] E. Smith, G. J. Nathan, and B. B. Dally, "The 'round jet inflow-condition anomaly' for the k-ε turbulence model," in *15th Australasian Fluid Mechanics Conference*, Sydney, NSW, Australia, 2004.

[58] G. Lipari and P. K. Stansby, "Review of experimental data on incompressible turbulent round jets," *Flow, Turbulence and Combustion*, vol. 87, no. 1, pp. 79–114, Mar. 2011, doi: https://doi.org/10.1007/s10494-011-9330-7.

[59] K. B. M. Q. Zaman, "Far-field noise of a subsonic jet under controlled excitation," *Journal of*

Fluid Mechanics, vol. 152, pp. 83–111, Mar. 1985, doi: https://doi.org/10.1017/s0022112085000581.

[60] J. Mi, M. Xu, and T. Zhou, "Reynolds number influence on statistical behaviors of turbulence in a circular free jet," *Physics of Fluids*, vol. 25, no. 7, pp. 075101–075101, Jul. 2013, doi: https://doi.org/10.1063/1.4811403.

[61] I. Namer and M. V. Ötügen, "Velocity measurements in a plane turbulent air jet at moderate Reynolds numbers," *Experiments in Fluids*, vol. 6, no. 6, pp. 387–399, Jan. 1988, doi: https://doi.org/10.1007/bf00196484.

[62] R. C. Deo, J. Mi, and G. J. Nathan, "The influence of Reynolds number on a plane jet," *Physics of Fluids*, vol. 20, no. 7, pp. 075108–075108, Jul. 2008, doi: https://doi.org/10.1063/1.2959171.

[63] D. R. Miller and E. W. Comings, "Force-momentum fields in a dual-jet flow," *Journal of Fluid Mechanics*, vol. 7, no. 2, pp. 237–256, Feb. 1960, doi: https://doi.org/10.1017/S0022112060001468.

[64] E. Tanaka, "The interference of two-dimensional parallel jets : 1st report, experiments on dual jet," *Bulletin of JSME*, vol. 13, no. 56, pp. 272–280, Jan. 1969, doi: https://doi.org/10.1299/jsme1958.13.272.

[65] E. Tanaka, "The interference of two-dimensional parallel jets : 2nd report, experiments on the combined flow of dual jet," *Bulletin of JSME*, vol. 17, no. 109, pp. 920–927, Jul. 1974, doi: https://doi.org/10.1299/jsme1958.17.920.

[66] K. Murai, M. Taga, and K. Akagawa, "An experimental study on confluence of two two-dimensional jets," *Bulletin of JSME*, vol. 19, no. 134, pp. 958–964, 1976, doi: https://doi.org/10.1299/jsme1958.19.958.

[67] T. L. Lim and T. B. Nickels, "Vortex rings," *Fluid Vortices*, vol. 30, pp. 95–153, Jan. 1995,

doi: https://doi.org/10.1007/978-94-011-0249-0_4.

[68] N. Fujisawa, K. Nakamura, and K. Srinivas, “Interaction of two parallel plane jets of different velocities,” *Journal of visualization*, vol. 7, no. 2, pp. 135–142, Apr. 2004, doi: https://doi.org/10.1007/bf03181586.

[69] A. Vouros and Th. Panidis, “Influence of a secondary, parallel, low Reynolds number, round jet on a turbulent axisymmetric jet,” *Experimental Thermal and Fluid Science*, vol. 32, no. 8, pp. 1455–1467, Sep. 2008, doi: https://doi.org/10.1016/j.expthermflusci.2008.03.007.

[70] X. K. Wang and S. K. Tan, “Experimental investigation of the interaction between a plane wall jet and a parallel offset jet,” *Experiments in Fluids*, vol. 42, no. 4, pp. 551–562, Feb. 2007, doi: https://doi.org/10.1007/s00348-007-0263-9.

[71] A. Kumar and M. K. Das, “Study of a turbulent dual jet consisting of a wall jet and an offset jet,” *Journal of Fluids Engineering*, vol. 133, no. 10, pp. 201-2011, Sep. 2011, doi: https://doi.org/10.1115/1.4004823.

[72] H. Wang, S. Lee, and Y. A. Hassan, “Particle image velocimetry measurements of the flow in the converging region of two parallel jets,” *Nuclear Engineering and Design*, vol. 306, pp. 89–97, Sep. 2016, doi: https://doi.org/10.1016/j.nucengdes.2015.09.032.

[73] H. Elbanna, S. Gahin, and I. Rashed, “Investigation of two plane parallel jets,” *AIAA Journal*, vol. 21, no. 7, pp. 986–991, Jul. 1983, doi: https://doi.org/10.2514/3.8187.

[74] S. Deng and M. J. Sheu, “Interaction of parallel turbulent plane jets,” *AIAA Journal*, vol. 29, no. 9, pp. 1372–1373, Sep. 1991, doi: https://doi.org/10.2514/3.10749.

[75] M. Ko and K. Y. Lau, “Flow structures in initial region of two interacting parallel plane jets,” *Experimental Thermal and Fluid Science*, vol. 2, no. 4, pp. 431–449, Oct. 1989, doi: https://doi.org/10.1016/0894-1777(89)90006-x.

[76] G. Marsters, “Interaction of two plane, parallel jets,” *AIAA Journal*, vol. 15, no. 12, pp. 1756–

1762, Dec. 1977, doi: https://doi.org/10.2514/3.60841.

[77] S. Zeierman, E. Gutmark, and N. Nosseir, "Characteristics of two adjacent rectangular jets," in *30th Aerospace Sciences Meeting and Exhibit,* Reno, NV, Jan. 1992, p.237.

[78] I. Moustafa, "Experimental investigation of high-speed twin jets," *AIAA Journal*, vol. 32, no. 11, pp. 2320–2322, Nov. 1994, doi: https://doi.org/10.2514/3.12293.

[79] T Harima, S. Fujita, and H. Osaka, "Turbulent properties of twin circular free jets with various nozzle spacing," *Engineering Turbulence Modelling and Experiments 6*, pp. 501–510, Jan. 2005, doi: https://doi.org/10.1016/b978-008044544-1/50048-0.

[80] B. Zang and T. H. New, "On the wake-like vortical arrangement and behaviour associated with twin jets in close proximity," *Experimental Thermal and Fluid Science*, vol. 69, pp. 127–140, Dec. 2015, doi: https://doi.org/10.1016/j.expthermflusci.2015.08.004.

[81] H. Helmholtz, "Über Integrale der hydrodynamischen Gleichungen, welche den Wirbelbewegungen entsprechen.," *Journal für die reine und angewandte Mathematik*, vol. 1858, no. 55, pp. 25–55, Jan. 1858, doi: https://doi.org/10.1515/crll.1858.55.25.

[82] W. B. Rogers, "On the formation of rotating rings by air and liquids under certain conditions of discharge," *American Journal of Science*, vol. 26, pp. 246–258, 1858.

[83] E. Reusch, "Ueber Ringbildung in Flüssigkeiten," *Annalen der Physik*, vol. 186, no. 6, pp. 309–316, Jan. 1860, doi: https://doi.org/10.1002/andp.18601860611.

[84] V. V. Meleshko and H. Aref, "A Bibliography of Vortex Dynamics 1858–1956," *Advances in Applied Mechanics*, vol. 41, pp. 197–292, Jan. 2007, doi: https://doi.org/10.1016/s0065-2156(07)41003-1.

[85] V. V. Meleshko, A. A. Gourjii, and T. S. Krasnopolskaya, "Vortex rings: history and state of the art," *Journal of Mathematical Sciences*, vol. 187, no. 6, pp. 772–808, Nov. 2012, doi: https://doi.org/10.1007/s10958-012-1100-0.

[86] P. G. Saffman, *Vortex Dynamics*. Cambridge ; New York: Cambridge University Press, 1995.

[87] M. Shusser and M. Gharib, "Energy and velocity of a forming vortex ring," *Physics of Fluids*, vol. 12, no. 3, pp. 618–621, Feb. 2000, doi: https://doi.org/10.1063/1.870268.

[88] D. T. New and S. C. H. Yu, *Vortex rings and jets: recent developments in near-field dynamics*. Singapore: Springer, 2015. doi: https://doi.org/10.1007/978-981-287-396-5.

[89] N. Didden, "On the formation of vortex rings: Rolling-up and production of circulation," *Zeitschrift für angewandte Mathematik und Physik ZAMP*, vol. 30, no. 1, pp. 101–116, Jan. 1979, doi: https://doi.org/10.1007/bf01597484.

[90] M. Gharib, E. Rambod, and K. Shariff, "A universal time scale for vortex ring formation," *Journal of Fluid Mechanics*, vol. 360, pp. 121–140, Apr. 1998.

[91] M. Rosenfeld, E. Rambod, and M. Gharib, "Circulation and formation number of laminar vortex rings," *Journal of Fluid Mechanics*, vol. 376, pp. 297–318, Dec. 1998, doi: https://doi.org/10.1017/s0022112098003115.

[92] W. Zhao, S. H. Frankel, and L. G. Mongeau, "Effects of trailing jet instability on vortex ring formation," *Physics of Fluids*, vol. 12, no. 3, pp. 589–596, Mar. 2000, doi: https://doi.org/10.1063/1.870264.

[93] K. Mohseni, H. Ran, and T. Colonius, "Numerical experiments on vortex ring formation," *Journal of Fluid Mechanics*, vol. 430, pp. 267–282, Mar. 2001, doi: https://doi.org/10.1017/s0022112000003025.

[94] D. E. Auerbach, "Stirring properties of vortex rings," *Physics of Fluids A: Fluid Dynamics*, vol. 3, no. 5, pp. 1351–1355, May 1991, doi: https://doi.org/10.1063/1.858064.

[95] D. Auerbach, "Some open questions on the flow of circular vortex rings," *Fluid Dynamics Research*, vol. 3, no. 1–4, pp. 209–213, Sep. 1988, doi: https://doi.org/10.1016/0169-5983(88)90067-6.

[96] K. Mohseni and M. Gharib, "A model for universal time scale of vortex ring formation," *Physics of Fluids*, vol. 10, no. 10, pp. 2436–2438, Oct. 1998, doi: https://doi.org/10.1063/1.869785.

[97] O. Pierrakos and P. P. Vlachos, "The effect of vortex formation on left ventricular filling and mitral valve efficiency," *Journal of Biomechanical Engineering*, vol. 128, no. 4, pp. 527–539, Aug. 2006, doi: https://doi.org/10.1115/1.2205863.

[98] J. Töger *et al.*, "Vortex ring formation in the left ventricle of the heart: analysis by 4D flow MRI and lagrangian coherent structures," *Annals of biomedical engineering*, vol. 40, no. 12, pp. 2652–2662, Jul. 2012, doi: https://doi.org/10.1007/s10439-012-0615-3.

[99] K. Zhang and D. E. Rival, "On the dynamics of unconfined and confined vortex rings in dense suspensions," *Journal of Fluid Mechanics*, vol. 902, p. A6, Nov. 2020, doi: https://doi.org/10.1017/jfm.2020.522.

[100] M. Cheng, J. Lou, and T. T. Lim, "Leapfrogging of multiple coaxial viscous vortex rings," *Physics of Fluids*, vol. 27, no. 3, p. 031702, Mar. 2015, doi: https://doi.org/10.1063/1.4915890.

[101] N. Riley and D. P. Stevens, "A note on leapfrogging vortex rings," *Fluid Dynamics Research*, vol. 11, no. 5, pp. 235–244, May 1993, doi: https://doi.org/10.1016/0169-5983(93)90114-p.

[102] A. J. Niemi, "Exotic statistics of leapfrogging vortex rings," *Physical Review Letters*, vol. 94, no. 12, Apr. 2005, doi: https://doi.org/10.1103/physrevlett.94.124502.

[103] K. Shariff and A. Leonard, "Vortex rings," *Annual Review of Fluid Mechanics*, vol. 24, no. 1, pp. 235–279, Jan. 1992, doi: https://doi.org/10.1146/annurev.fl.24.010192.001315.

[104] T. Fohl and J. S. Turner, "Colliding vortex rings," *Physics of Fluids*, vol. 18, no. 4, p. 433, 1975, doi: https://doi.org/10.1063/1.861169.

[105] S. Kida, M. Takaoka, and F. Hussain, "Collision of two vortex rings," *Journal of Fluid Mechanics*, vol. 230, pp. 583–646, Sep. 1991, doi:

https://doi.org/10.1017/s0022112091000903.

[106] T. L. Lim and T. B. Nickels, “Instability and reconnection in the head-on collision of two vortex rings,” *Nature*, vol. 357, no. 6375, pp. 225–227, Sep. 1992, doi: https://doi.org/10.1038/357225a0.

[107] J. R. Mansfield, I. Hoteit, and C. Meneveau, “Dynamic LES of colliding vortex rings using a 3D vortex method,” *Journal of Computational Physics*, vol. 152, no. 1, pp. 305–345, Jun. 1999, doi: https://doi.org/10.1006/jcph.1999.6258.

[108] Y. Oshima, “Head-on collision of two vortex rings,” *Journal of the Physical Society of Japan*, vol. 44, no. 1, pp. 328–331, Jan. 1978, doi: https://doi.org/10.1143/jpsj.44.328.

[109] S. C. Crow, “Stability theory for a pair of trailing vortices,” *AIAA Journal*, vol. 8, no. 12, pp. 2172–2179, Dec. 1970, doi: https://doi.org/10.2514/3.6083.

[110] W. T. Ashurst and D. I. Meiron, “Numerical study of vortex reconnection,” *Physical Review Letters*, vol. 58, no. 16, pp. 1632–1635, Apr. 1987, doi: https://doi.org/10.1103/physrevlett.58.1632.

[111] S. Kida, M. Takaoka, and F. Hussain, “Reconnection of two vortex rings,” *Physics of Fluids A: Fluid Dynamics*, vol. 1, no. 4, pp. 630–632, Apr. 1989, doi: https://doi.org/10.1063/1.857436.

[112] H. Aref and I. Zawadzki, “Linking of vortex rings,” *Nature*, vol. 354, no. 6348, pp. 50–53, Nov. 1991, doi: https://doi.org/10.1038/354050a0.

[113] S. Kida and M. Takaoka, “Vortex reconnection,” *Annual Review of Fluid Mechanics*, vol. 26, no. 1, pp. 169–177, Jan. 1994, doi: https://doi.org/10.1146/annurev.fl.26.010194.001125.

[114] I. D. Sullivan, J. Niemela, R. E. Hershberger, D. Bolster, and R. J. Donnelly, “Dynamics of thin vortex rings,” *Journal of Fluid Mechanics*, vol. 609, pp. 319–347, Aug. 2008, doi: https://doi.org/10.1017/s0022112008002292.

[115] P. S. Krueger and M. Gharib, "The significance of vortex ring formation to the impulse and thrust of a starting jet," *Physics of Fluids*, vol. 15, no. 5, pp. 1271–1281, Apr. 2003, doi: https://doi.org/10.1063/1.1564600.

[116] J. J. Allen and B. Auvity, "Interaction of a vortex ring with a piston vortex," *Journal of Fluid Mechanics*, vol. 465, pp. 353–378, Aug. 2002, doi: https://doi.org/10.1017/S0022112002001118.

[117] "Particle Image Velocimetry (PIV)," *Dantec Dynamics*, 2019. https://www.dantecdynamics.com/wp-content/uploads/2019/11/particle-image-velocimetry-poster-1.pdf

[118] R. D. Keane and R. J. Adrian, "Optimization of particle image velocimeters: II. Multiple pulsed systems," *Measurement Science and Technology*, vol. 2, no. 10, pp. 963–974, Oct. 1991, doi: https://doi.org/10.1088/0957-0233/2/10/013.

[119] R. D. Keane and R. J. Adrian, "Theory of cross-correlation analysis of PIV images," *Applied Scientific Research*, vol. 49, no. 3, pp. 191–215, Jul. 1992, doi: https://doi.org/10.1007/bf00384623.

[120] R. J. Keane and R. J. Adrian, "Optimization of particle image velocimeters. I. Double pulsed systems," *Measurement Science and Technology*, vol. 1, no. 11, pp. 1202–1215, Nov. 1990, doi: https://doi.org/10.1088/0957-0233/1/11/013.

[121] R. J. Adrian, J. Westerweel, and Cambridge University Press, *Particle image velocimetry*. Cambridge: Cambridge University Press, Cop, 2011.

[122] A. Fincham and G. Delerce, "Advanced optimization of correlation imaging velocimetry algorithms," *Experiments in Fluids*, vol. 29, no. 7, pp. S013–S022, Dec. 2000, doi: https://doi.org/10.1007/s003480070003.

[123] F. Scarano and M. L. Riethmuller, "Advances in iterative multigrid PIV image processing,"

Experiments in Fluids, vol. 29, no. 7, pp. S051–S060, Dec. 2000, doi: https://doi.org/10.1007/s003480070007.

[124] A. Melling, "Tracer particles and seeding for particle image velocimetry," *Measurement Science and Technology*, vol. 8, no. 12, pp. 1406–1416, Dec. 1997, doi: https://doi.org/10.1088/0957-0233/8/12/005.

[125] J. Westerweel, "Analysis of PIV interrogation with low-pixel resolution," *Optical Diagnostics in Fluid and Thermal Flow*, pp. 624–635, Dec. 1993, doi: https://doi.org/10.1117/12.163745.

[126] J. Westerweel, "Efficient detection of spurious vectors in particle image velocimetry data," *Experiments in Fluids*, vol. 16–16, no. 3–4, pp. 236–247, Feb. 1994, doi: https://doi.org/10.1007/bf00206543.

[127] J. Westerweel and F. Scarano, "Universal outlier detection for PIV data," *Experiments in Fluids*, vol. 39, no. 6, pp. 1096–1100, Aug. 2005, doi: https://doi.org/10.1007/s00348-005-0016-6.

[128] J. Duncan, D. Dabiri, J. Hove, and M. Gharib, "Universal outlier detection for particle image velocimetry (PIV) and particle tracking velocimetry (PTV) data," *Measurement Science and Technology*, vol. 21, no. 5, p. 057002, Mar. 2010, doi: https://doi.org/10.1088/0957-0233/21/5/057002.

[129] V. Holmen, "Methods for vortex identification," *Master's Theses in Mathematical Sciences*, 2012.

[130] B. Epps, "Review of vortex identification methods," in *55th AIAA Aerospace Sciences Meeting*, Grapevine, Texas, Jan. 2017.

[131] P. Chakraborty, S. Balachandar, and R. J. Adrian, "On the relationships between local vortex identification schemes," *Journal of Fluid Mechanics*, vol. 535, pp. 189–214, Jul. 2005, doi:

https://doi.org/10.1017/s0022112005004726.

[132] Y. Wu and K. T. Christensen, “Population trends of spanwise vortices in wall turbulence,” *Journal of Fluid Mechanics*, vol. 568, pp. 55–55, Dec. 2006, doi: https://doi.org/10.1017/s002211200600259x.

[133] Q. Chen, Q. Zhong, X. Wang, and D. Li, “An improved swirling-strength criterion for identifying spanwise vortices in wall turbulence,” *Journal of Turbulence*, vol. 15, no. 2, pp. 71–87, Feb. 2014, doi: https://doi.org/10.1080/14685248.2014.881488.

[134] R. Camussi, “Coherent structure identification from wavelet analysis of particle image velocimetry data,” *Experiments in Fluids*, vol. 32, no. 1, pp. 76–86, Jan. 2002, doi: https://doi.org/10.1007/s003480200008.

[135] A. Rinoshika and H. Rinoshika, “Application of multi-dimensional wavelet transform to fluid mechanics,” *Theoretical and Applied Mechanics Letters*, vol. 10, no. 2, pp. 98–115, Jan. 2020, doi: https://doi.org/10.1016/j.taml.2020.01.017.

[136] S. Sadeqi, N. Xiros, S. Rouhi, J. Ioup, J. Van Zwieten, and C. Sultan, “Wavelet transformation analysis applied to incompressible flow field about a solid cylinder,” in *Proceesing of 5-6th Thermal and Fluids Engineering Conference (TFEC)*, New Orleans, LA, 2021, pp. 353–363.

[137] M. van Berkel, G. Witvoet, P. Nuij, and M. Steinbuch, *Wavelets for feature detection : theoretical background*, Eindhoven (Netherlands): CST, 2010.

Appendix

A - Velocity fields and vorticity contours for different stroke ratios and nozzle spacings

Nozzle spacing $S/D_0 = 1.74$

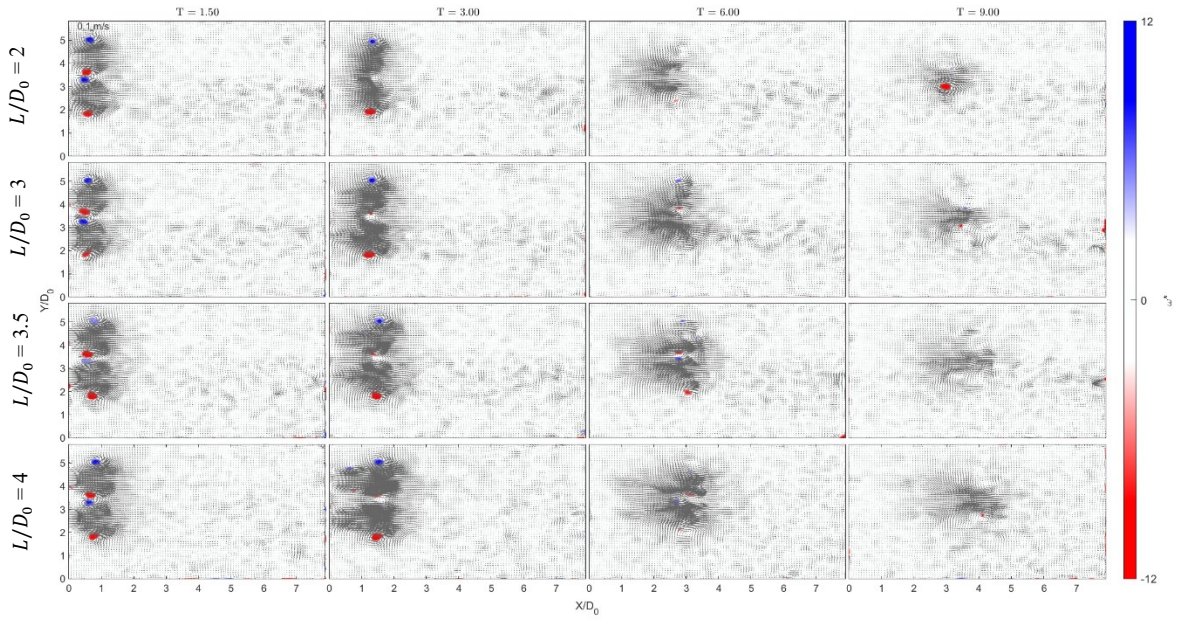

Nozzle spacing $S/D_0 = 1.97$

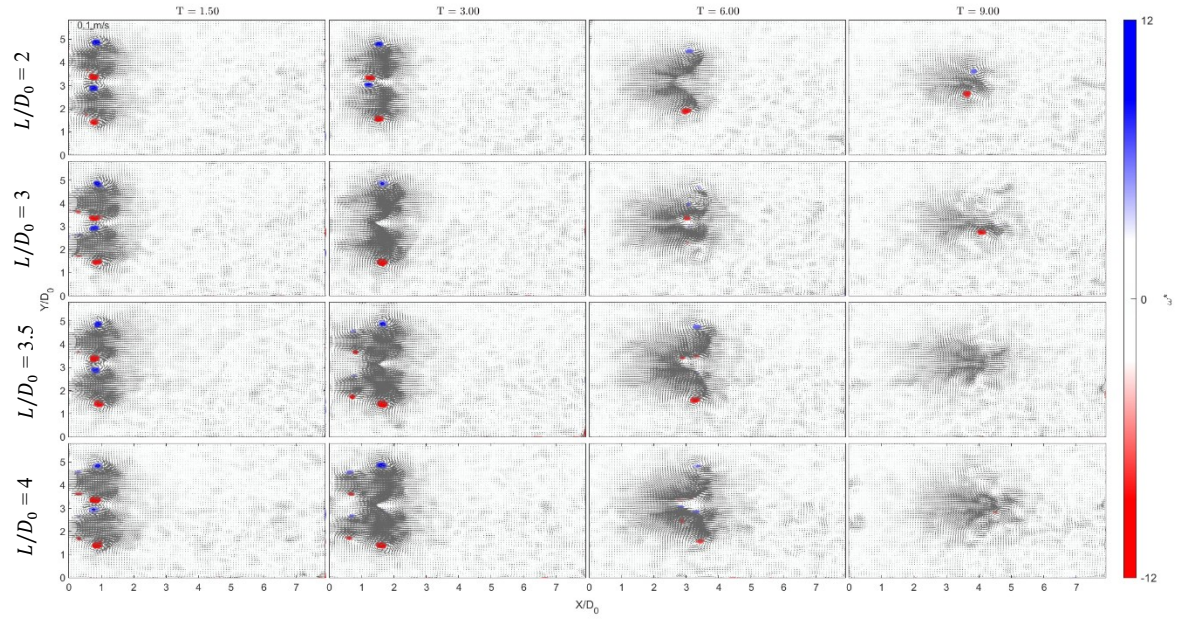

Nozzle spacing S/D_0 = 2.45

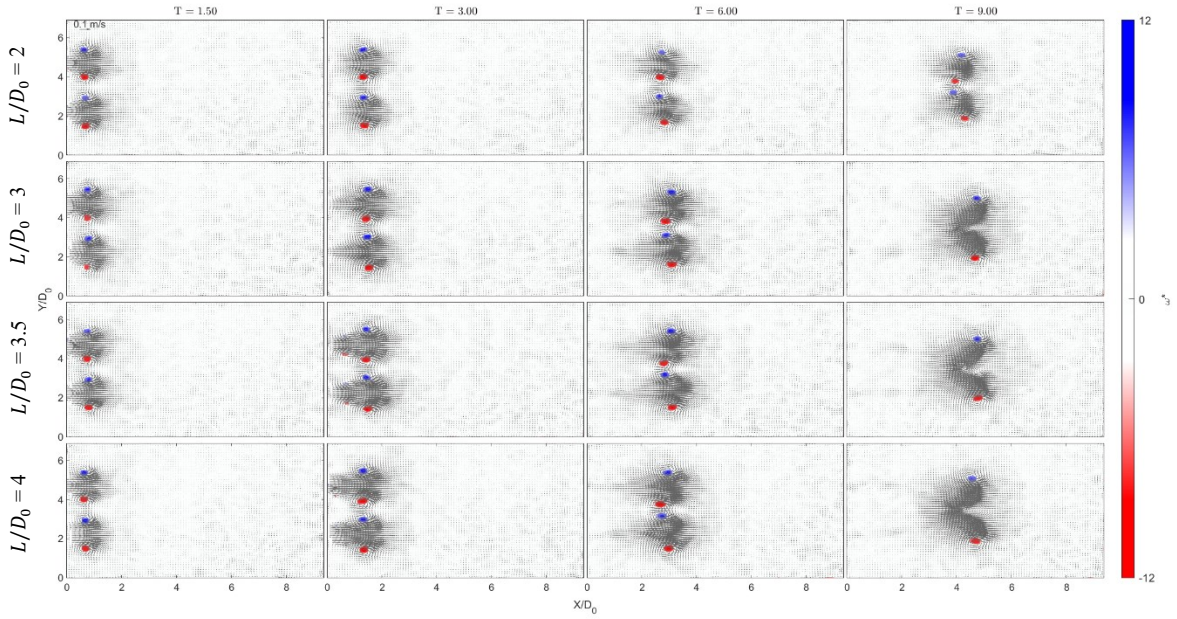

Nozzle spacing S/D_0 = 2.82

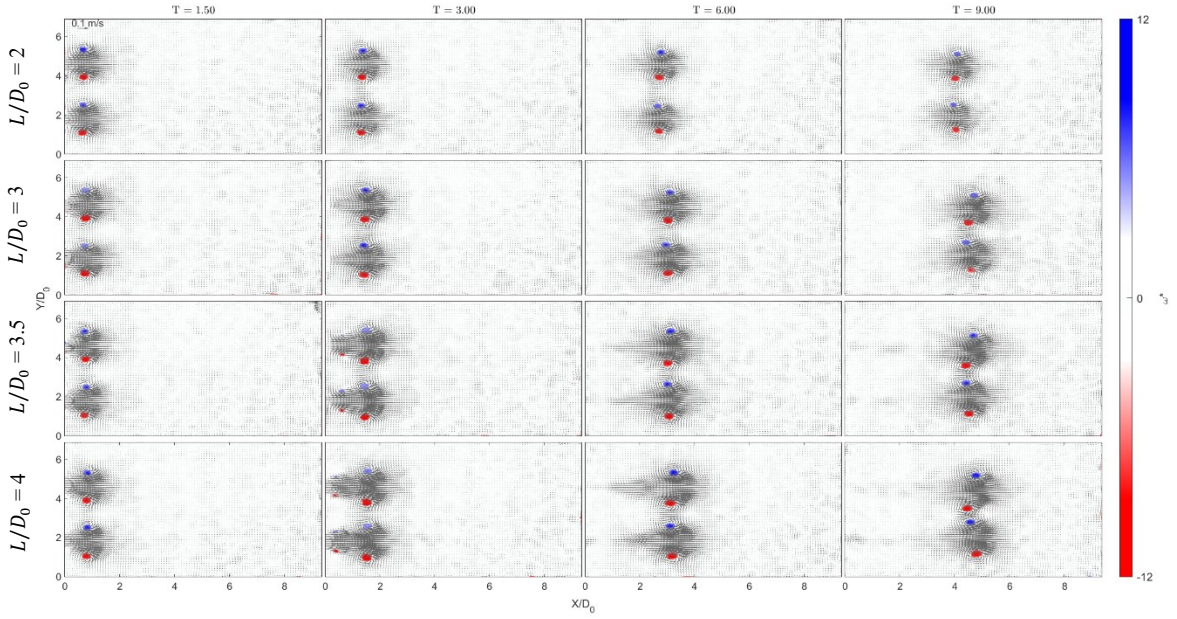

B – Vorticity of the vortex cores

Nozzle spacing S/D_0 = 3.20, stroke ratio L/D_0 = 2

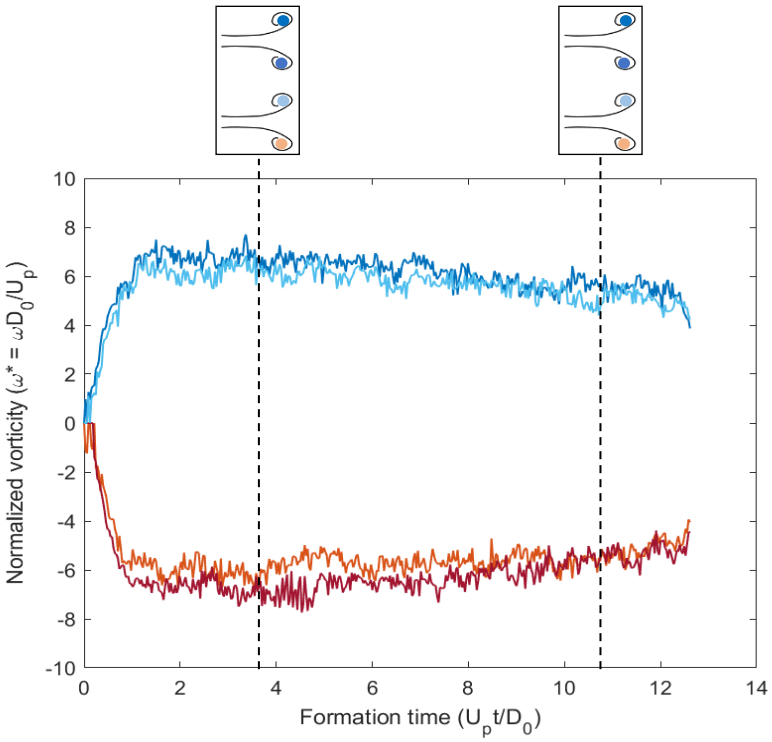

Nozzle spacing S/D_0 = 1.49, stroke ratio L/D_0 = 2